Refining Gondwana and Pangea palaeogeography: estimates of Phanerozoic non-dipole (octupole) fields

Trond H. Torsvik[1] and Rob Van der Voo[2]

[1]*VISTA, c/o Geodynamic Centre, NGU, Leiv Eiriksonsvei 39, N-7491 Trondheim & Institute for Petroleum Technology and Applied Geophysics, S.P. Andersens v.* 15a, N-7491 *NTNU, Norway. E-mail: trond.torsvik@ngu.no*
[2]*Department of Geological Sciences, University of Michigan, Ann Arbor,* MI 48109-1063, *USA*

SUMMARY

Reliable Phanerozoic paleopoles have been selected from the stable parts of the Gondwana continents and, upon appropriate reconstruction, have been combined in an apparent polar wander (APW) path, which can be compared with a previously compiled path for Laurussia. This comparison once again confirms that Pangea-A reconstructions for Late Palaeozoic and early Mesozoic times cannot be reconciled with the available paleomagnetic data, unless these data are corrected for latitudinal errors caused by non-dipole (octupole) field contributions or by inclination shallowing. Because the discrepancies persist even when only paleopoles from igneous rocks are used, inclination shallowing cannot be the sole cause of the problem. There is an apparent decrease in the percentage of octupole field contributions needed as a function of time; for Mesozoic and younger time, Gondwana–Laurussia comparisons require, on average, lower ratios of octupole/dipole fields than for Palaeozoic time. However, the Gondwana paleopoles for the Palaeozoic include a much greater proportion of results derived from sedimentary rocks than do those for the Mesozoic, so that this apparently diminishing octupole field contribution may be an artefact. We have also examined whether the clustering of coeval Gondwana poles improves with optimal G3 contributions, but found that while there are improvements, they are not systematic and not statistically significant. A combined APW path has been constructed for Pangea for times since the Mid-Carboniferous, which accounts for octupole fields, or equivalently, inclination shallowing. We argue that this 'global' path is an improvement over previous constructions as it represents a self-consistent plate tectonic model and does not violate widely accepted Pangea-A reconstructions.

Key words: apparent polar wander, Gondwana, inclination shallowing, non-dipole field, octupole, palaeogeography, palaeomagnetism, Pangea.

1 INTRODUCTION AND RATIONALE

Palaeomagnetic poles are calculated with the fundamental assumption that the time-averaged geomagnetic field is that of a geocentric axial dipole (GAD), but a number of recent studies have cast doubts on this fundamental assumption (Kent & Smethurst 1998; Van der Voo & Torsvik 2001; Torsvik *et al.* 2001a; Si & Van der Voo 2001). These authors argue for long-term non-dipole (octupole) field contributions of the order of 6–25 per cent of the total field in Phanerozoic and Precambrian times. These values imply latitudinal errors as high as 525–1760 km in palaeomagnetic reconstructions (if poles are calculated using the GAD formula). Combined with a typical analytical precision of 300–500 km at best, this raises serious concerns concerning the resolution of palaeomagnetic reconstructions. It is therefore of paramount importance to determine the amount of ancient non-dipole field components, notably because palaeomagnetism is the only method that provides quantifiable plate reconstructions prior to the Mid-Jurassic.

It is comparatively unproblematic to estimate non-dipole field components for the last few million years because the effects of relative plate movements are unimportant. For the last 5 Myr, the time-averaged field deviates from that of a pure GAD, with quadrupole ($G2 = g_2^0/g_1^0$) and octupole ($G3 = g_3^0/g_1^0$) field contributions ranging from 3 to 9 per cent (McElhinny *et al.* 1996), but the statistical significance of some of these estimates at the 95 per cent confidence level is arguable.

Estimating non-dipole field components for ancient times is much more difficult: (1) Kent & Smethurst (1998) evaluated the distribution of Precambrian and Palaeozoic inclinations and found that a persistent octupolar contribution of 25 per cent (G3 = 0.25) best fitted the data. Alternatively, they proposed that a bias of shallow inclinations could reflect a tendency of continents to be cycled into equatorial belts because

supercontinents (e.g. Rodinia and Pangea) may trigger true polar wander. (2) Van der Voo & Torsvik (2001) devised a new method for estimating non-dipole fields and estimated an average octupole field of 10 per cent (G3 = 0.1) from Carboniferous to Early Tertiary times. (3) Torsvik *et al.* (2001a) found that systematic discrepancies between the hotspot and palaeomagnetic reference schemes between 40 and 95 Ma could be reconciled with a long-term, octupole field contribution (G3 = 0.08). (4) Si & Van der Voo (2001) compared Tertiary paleolatitudes in central Asia with those predicted from Eurasia, and found that a well-known palaeolatitude discrepancy was eliminated with G3 > 0.06.

There is a misfit between palaeomagnetic results from Laurussia and Gondwana in a classical Pangea-A configuration (Van der Voo 1993), and Van der Voo & Torsvik (2001) demonstrated how this Late Palaeozoic and Early Mesozoic enigma could arise from octupole field contributions. In this paper we present a more complete analysis for the Gondwana continents and its bearing on the Pangea problem. We first start with a comprehensive review of the Gondwanan palaeomagnetic data base, and then compare the results with Laurussia.

2 DATA SELECTION AND RECONSTRUCTION FITS

Gondwana was assembled at around 550 Ma (Meert & Van der Voo 1997) and became embedded in the Pangea Supercontinent during the Carboniferous. Pangea breakup commenced during the Mid-Jurassic with the opening of the Central Atlantic. In this account we have compiled palaeomagnetic poles from Gondwana core elements (Africa, South America, Madagascar, Greater India, Cratonic Australia and East Antarctica), including data not only from its Vendian formation to Mid-Jurassic dispersal, but also post-break-up data through the Cretaceous–Tertiary boundary (Table 1).

As a starting point we included poles listed in Van der Voo (1993) with a quality factor $Q \geq 3$, but have upgraded the data base with newer poles, and with revised ages according to timescales from Tucker & McKerrow (1995), Tucker *et al.* (1998) and Gradstein *et al.* (1995). The numerical ages of several poles have been adjusted in view of more recent and precise isotope ages, wherever we encountered such information.

Fig. 1 shows the sampling locations of the accepted palaeomagnetic poles on a Permian-aged Gondwana reconstruction with Africa held fixed. The poles can be identified by their ages (Table 1). We also show an age–frequency distribution diagram in Fig. 2: Cambrian through Early Ordovician, the Permo-Carboniferous, the Jurassic and the Late Cretaceous epoch are well represented, whilst there are few poles from the Mid-Ordovician through to the Early Carboniferous, for the Triassic, and for Early Cretaceous times.

Gondwana–Pangea fits and subsequent dispersal histories follow Lottes & Rowley (1990) and Müller *et al.* (1993, 1997), with some minor modifications. We maintain relatively tight fits for Permian and older times (pre-drift), and in our analysis fits were interpolated down to 1 Ma to allow a direct comparison with the age of the palaeomagnetic poles. Fits are listed in 10 Ma intervals in Table 2. We initially contemplated refining these fits, if possible, by comparing palaeomagnetic data from periods with good data coverage in a similar fashion to a recent analysis for Laurussia (Torsvik *et al.* 2001c), but there are some obstacles attached to undertaking a similar analysis for Gondwana. The Gondwana data sets are generally not as robust as North American–European data sets, but, more importantly, while uncertainties in the fit between North America–Europe are dominantly east–west and therefore orthogonal to the effects of zonal non-dipole fields, uncertainties in palaeomagnetic reconstruction fits for Gondwana elements cannot always be distinguished from zonal non-dipole fields. In simple terms—if we first estimate 'best-fits' using palaeomagnetic poles calculated from the geocentric dipole formulae and later argue for substantial zonal non-dipole fields (as we indeed do in this paper), these fits would deteriorate and not be relevant. Admittedly, we are not entirely satisfied with published Gondwana fits, notably where estimates of pre-drift extension in parts of SE Gondwana and India–Madagascar fits (see Torsvik *et al.* 2000) are involved, but a possible refinement of the fits is of secondary importance in the following discussion.

2.1 Africa

Following Van der Voo (1993) we have divided Africa into three tectonic domains, South Africa, NE Africa and NW Africa. We use reconstruction parameters of Lottes & Rowley (1990) and use transitional fits between 130 and 100 Ma (Table 2).

We include 22 poles (547–90 Ma) from South Africa (Figs 1 and 3a) with most poles being of Late Carboniferous to Late Cretaceous age; we list only five reliable poles from latest Vendian to Devonian times (Table 1). The Early Cretaceous Kaoko lavas (Namibia) are associated with the initial opening of the South Atlantic, and the subsequent separation of Africa from South America at around 130 Ma.

Eleven poles from NE Africa are mostly Late Cretaceous in age (Fig. 3b). In addition, we include two poles of Carboniferous and Devonian age and the Ordovician-aged Salala Ring Complex pole from Sudan. The latter pole is somewhat problematic—it is one of the few Mid-Ordovician poles from the Gondwana data sets but it is rather different from poles of both older and younger age.

Thirty-one poles, all of earliest Devonian and younger age, have been included in our compilation for NW Africa (Fig. 3c). The Air Intrusives is the only Early Devonian pole in the entire Gondwana data set and hence is of paramount importance in the apparent polar wander (APW) path that we generate later.

2.2 Madagascar

Madagascar was located next to East Africa from latest Precambrian (Gondwana) to Mesozoic (Pangea) times. Mesozoic separation of Africa and Madagascar was preceded by a long period of continental rifting that generated Upper Carboniferous through Mid-Jurassic basins (Karoo

Table 1. Selected palaeomagnetic data (quality factor $Q \geq 3$; Van der Voo 1993) from core Gondwana elements.

Continent, formation, country	Q	α_{95}	Location		Pole		Age	Ref. no
			Lat.	Long.	Lat.	Long.		
South Africa (Fig. 3a)								
Cretaceous Kimberlites 1, South Africa, Lesotho	5	5.2*	−29	26	−64.1	46.1	90	2293
Lupata Series Volcanics, Mozambique	4	3	−16.7	34.2	−61.8	79.5	111	992
Mlanje Massif Syenite, Malawi	3	9.3	−16	35.6	−60	82	124	401
Cretaceous Kimberlites 2, South Africa	6	9.7*	−28.5	24	−47.6	89.9	129	2293
Kaoko lavas, Namibia	5	3.1	−20	14	−48.3	86.6	132	126
Hoachanas Lavas, Namibia	3	15.8	−24	18	−61.9	71.9	171	126
Stormberg Lavas, South Africa, Lesotho	5	3.2	−29.3	28.6	−71.6	93.5	180	3090
Stormberg Lavas, Sani Pass-Maseru, Lesotho	4	11	−29.5	28.5	−70.5	88.7	180	984
Marangudzi Ring Complex, Zimbabwe	5	8.7	−22.1	30.7	−70.7	106.7	186	470
Karroo Lavas, Zimbabwe, Mozambique	3	7	−18	30	−57	84	193	635
Karroo Dolerites, South Africa, Zimbabwe	5	9.5	−24	31	−65.4	75.1	193	317
Red Sandstone Formation, Zambia	3	4.6	−16.2	28.8	−68	50.5	221	323
Cassanje Series, Angola	3	6	−10	17.5	−54	80	248	1960
Permian Redbeds, Tanzania	4	5.3	−8.5	35.4	−26.9	85.1	254	2736
K3 Beds, Galula coalfield, Tanzania	3	5	−8.8	32.9	−46	40	257	324
K3 Beds, Songwe-Ketewaka, Tanzania	3	12	−10	34.5	−27.6	89.8	257	324
K1 Dwyka Varves, Zimbabwe, Zambia, Tanzania	6	5.6	−13.5	30	−26.5	26.5	281	435
Bokkeveld Group, Cape Province, South Africa	4	7	−33.5	19	10	15	398	1416
Pakhuis, Cedarberg Formations, South Africa	5	18	−33	19.5	25	343	446	1416
Graafwater Formation, South Africa	6	9	−34.1	18.4	28	14	482	1416
Ntonya Ring Structure, Malawi	5	1.9	−15.5	35.3	27.5	344.8	522	404
Sinyai Dolerite, Kenya	4	5	0.5	37.1	−28.4	319.1	547	3106
Northeast Africa (Fig. 3b)								
Dakhla Shales, Gebel Gifita, Egypt	4	8.5	25.5	29	−81.5	45	74	1510
Quseir Trachytes, Egypt	5	3.1	26	34	−63	72.3	77	3260
East El Oweinat Volcanics, Egypt	4	12.5	23.2	29.5	−67.8	88.8	81	1265
El Khafa Ring Complex, Egypt	4	7.5	24.1	34.7	−61.1	57.6	84	3260
Nubian Sandstone-Volcanics, Egypt	3	5.6	24.5	34.2	−63.5	37.9	87	114
Abu Khrug Ring Complex, Egypt	5	12.9	24.6	34	−59.1	86	89	3260
Wadi Natash Volcanics, Egypt	5	8.5	24.4	34.3	−69.3	78.1	93	1500
Wadi Natash Volcanics, Egypt	3	18.1	24.5	33.5	−75.7	48.3	94	3260
Abu Durba Sediments, SW Sinai, Egypt	3	7.2	29.5	34.5	−25.6	64	306	2784
Gilif Hills Volcanics, Bayuda Desert, Sudan	3	10.8	17.8	32.7	25.9	11.6	377	2189
Salala Ring Complex, Sudan	6	9.2	21.4	36.1	39.6	329.5	463	2715
Northwest Africa (Fig. 3c)								
Basalts Series I, Fuerteventura, Spain	4	4.4	28.6	345.9	−68.8	40.8	76	1493
Basalt Series I, Gran Canaria, Tenerife, Spain	5	8	28.1	343.5	−72	71.2	81	1122
Intrusives, Morocco, Beni Mellal, Morocco	4	14	32.5	354	−46	78	120	1859
Upper Jurassic sediments, Tunisia	6	6.3	36.2	10	−65.2	20.3	152	1167
Intrusive rocks, Nigeria	3	19.2	9	8.6	−62.5	61.6	160	1081
Beni Mellal Basalts, Morocco	4	11	32.5	354	−45	68	173	1859
Beni Mellal Volcanics, Morocco	6	9	32.2	354	−44	71	173	125
Morrocan Intrusives, Morocco	3	0	32	352.5	−71	36	183	148
Diabase dykes and sills, Liberia	5	7.4	6.5	349.5	−68.5	62.4	185	140
Hank Volcanics, North Mauritania	4	4.1	24	353	−69.4	52	187	3259
Hodh Volcanics, South Mauritania	4	6.1	17	352	−71.4	60.2	187	3260
Freetown Complex, Sierra Leone	4	6.2	8.3	346.8	−82.9	32.7	193	3287
Zarzaitine Formation, Algeria	6	2.6	27.9	9.3	−70.9	55.1	206	2932
Argana Redbeds, Morocco	3	12	30.5	351	−50.6	71.4	221	1080
Upper Triassic Sediments, Southern Tunisia	3	11.5	33	10.6	−54.9	43.3	221	3020
Djebel Tarhat Redbeds, Morocco	3	7.8	33.5	353	−24	63.8	273	1080
Serie d'Abadla, Upper Unit, Morocco	5	6	31	357.3	−29	60	273	1459
Taztot Trachyandesite, Morocco	3	4.6	32.2	354	−38.7	56.8	273	723
Northwest Africa (Fig. 3c)								
Chougrane Redbeds, Morocco	5	4.7	33	353.7	−32.2	64.1	273	723
Abadla Formation Lower Unit, Algeria	5	3.6	31.2	357.3	−29.1	57.8	275	3275
Volcanics, Mechra Abou-Chougrane, Morocco	3	20.9	32.5	352.5	−36	58	280	1859
Upper El Adeb Larache Formation, Algeria	5	2.8	27.5	8.9	−38.5	57.5	286	2540
Lower Tiguentourine Formation, Algeria	4	4.1	27.7	9	−33.8	61.4	290	2728
Lower El Adeb Larache Formation, Algeria	5	3.5	27.5	8.9	−28.7	55.8	307	2540
Ain Ech Chebbi, Hassi Bachir Form., Algeria	4	4.1	26.6	1	−25.4	54.8	316	1629

Table 1. (*Continued.*)

Continent, formation, country	Q	α_{95}	Location Lat.	Location Long.	Pole Lat.	Pole Long.	Age	Ref. no
Reggane Basin, Mid-Carboniferous,	6	5.3	26.6	0.3	−26.6	44.7	320	#1
Beni-Zireg Limestones, Algeria	6	3.7	31.9	358.2	−19.2	19.8	365	2521
Griotte Limestones, Algeria	5	3.7	30	358	−21	19.9	365	2725
Hazzel Matti Formation, North Ahaggar, Algeria	5	6.3	24.9	2.1	−16.2	61.7	379	2884
Air intrusives, Niger, West Africa	5	6.6	19.3	8.8	−43.4	8.6	409	1364
Madagascar (Fig. 3d)								
Volcanics, Mailaka Andria	4	6.9	−18	44.4	−70.3	63.1	87	708
Volcanics, Antanimena Andria	4	4.9	−16.4	46	−66.1	49.7	87	708
Volcanics, Massif d'Androy Andria	4	7.6	−24.2	46	−64	63	87	547
Volcanics, Southeast Coast Andria	4	4.4	−21.8	48	−65.8	35.6	87	708
Volcanics, Mangoky-Anilahy Andria	4	8.9	−22.8	44.3	−73.7	73.1	87	708
Dolerites, East Madagascar	5	4.3	−18	47	−65.5	38	87	#2
Dolerites, Tamatave Andria	3	2.8	−18	47	−60.2	32.1	87	708
Volcanics, SW Madagascar	6	2.4	−23.2	44.3	−76.8	68.2	87	3210
Isalo Group	3	5.9	−18	45.5	−74	97.1	206	147
Sakamena Group	3	7.6	−23.3	44.5	−76.7	110.8	250	#3
Sakoa Group	3	9.5	−23.7	44.6	−51.3	72.6	305	#3
Carion Granite	5	11	−19	47.7	−6.8	1	509	#4
India (Fig. 3e)								
Mt Pavagarh Traps, Gujrat	4	5.4	22.5	73.5	−39.2	105.6	64	94
Deccan traps, Dhar region	3	6.5	22.4	75.4	−29	113	65	1168
Deccan Dyke Swarms, Western India	5	9.4	21.5	74.3	−37.2	100.5	65	3094
Deccan Traps, Amboli	4	10.2	15.9	74.3	−41.4	79.9	65	107
Deccan Traps, Malwa Plateau	3	13.2	22.5	75.8	−36.3	90.4	65	687
Deccan Traps, Mahabaleshwar	4	6.7	17.9	73.6	−40	96	65	107
Deccan Traps–Nagpur to Bombay traverse	6	5.9	20	75	−38.4	102.4	65	393
Deccan Traps, Western Ghats, Near Poona	3	3.8	17.8	73.8	−34.5	103.6	65	705
Deccan Traps, Jalna	3	3.8	19.9	75.9	−39	99	65	686
Central Kerala Dykes	4	10.1	9.7	76.7	−34.6	94	69	2754
Central Kerala Gabbro Dyke	4	12	9.7	76.7	−21.6	119.4	88	2754
St Mary Island Rhyolites	5	7.5	13.4	74.7	−14.2	117.8	91	#5
Rajmahal Traps, Bihar	6	3.5	24.6	87.7	−7	117	116	678
Rajmahal Traps, West Bengal and Bihar	3	4	24.7	87.6	−3	118	116	633
Rajmahal Traps, West Bengal	6	8.3	25	87.4	−9.3	124.8	116	2977
Sylhet Traps, Khasi Hills	3	7	25	91	−16	121	116	985
Rajmahal Traps, Bihar	5	2.4	24.7	87.7	−9.4	116.6	117	3095
Pachmarhi Beds, Central India	5	4.6	22.4	78.4	−10.1	130.1	206	593
Mangli Beds, Central India	4	4.6	20.5	79	7.3	124.3	243	593
Panchet clays, Karanpura Coalfields	5	6	23.8	85.3	7.5	120.5	248	162
Kamthi Redbeds, Wardha Valley	6	6.5	20	79	4	129	250	163
Kamthi Beds, Tadoba	3	1.8	20.2	79.3	4.1	102.8	250	593
Upper Bhander Sandstones	4	5.5	26.6	77.7	−48.5	33.5	540*	212
Rewa Sandstones, Vindhyan System	3	13.7	23.8	78.9	−35	42	545*	254
Bhander and Rewa Series, U. Vindhyan System	3	11.1	27	77.5	−51	37.8	545*	1084
*uncertain—most likely Early Cambrian								
Pakistan (Fig. 3e)								
Wargal and Chhidru Formations, Salt Range	6	4.3	32.6	71.8	2.2	125.8	250	2467
Alozai Formation, Baluchistan	3	12.1	30	66.9	18.1	111	289	1236
Salt Pseudomorph Beds, Salt Range	4	5.9	32.7	73	−26.6	33.5	511	209
Pakistan (Fig. 3e)								
Jutana Formation, Saidu Valley	4	11	32.2	71	−20.5	51	520	1412
Purple Sandstone, Salt Range	3	12	32.7	73	−28	32	535	577
South America (Fig. 3d)								
Rio de Los Molinos dykes 1, Cordoba, Argentina	3	6	−31.8	295.5	−77	18	65	102
Patagonian Plateau Basalts, Chile, Argentina	6	4.3	−45.3	288.7	−78.7	358.4	71	2374
Itatiaia and Passa Quatro Complexes, SE Brazil	5	5.9	−22.4	315.2	−79.5	0	72	3261
Volcanic Hills, San Luis and Cordoba, Argentina	4	13	−33	295	−70.2	44.5	75	1180
Sao Sabastiao Island Intrusions, SE Brazil	5	4.2	−23.8	316.7	−79.4	331.9	80	3261
Pocos de Caldas Alkaline Complex, SE Brazil	6	2.6	−21.8	313.5	−83.2	320.1	83	3261
Intrusives, Cabo de Santo Agostinho, Brazil	3	4.8	−8.4	325	−87.6	315.1	92	1448
Pirgua basalts and redbeds, Argentina	4	8	−25.8	294.2	−85	222	95	1131
East Maranhao Intrusives, Brazil	4	2.8	−6.5	318	−83.6	81	118	1431

Table 1. (*Continued.*)

Continent, formation, country	Q	α_{95}	Location Lat.	Location Long.	Pole Lat.	Pole Long.	Age	Ref. no
Serra Geral Basalts, Brazil	4	3.7	−29	310	−84.6	115.4	119	765
Vulcanitas Cerro Colorado, Cordoba, Argentina	3	10.4	−32	296	−81	14	121	123
Florianopolis Dyke Swarm, Brazil	6	2.6	−27.7	311.5	−89.1	3.3	123	3190
El Salto-Almafuerte Lavas, Argentina	5	5.9	−32.2	295.8	−72	25	124	1087
Ponta Grossa Dykes, Brazil	6	2	−24.5	310	−82.4	30.3	131	2958
Rio de Los Molinos dykes 2, Cordoba, Argentina	3	11	−31.8	295.5	−79	8	139	102
Dykes, Rio Grande do Norte, NE Brazil	4	14.1	−5.7	323.6	−80.6	275	146	1509
Chon Aike Formation, Argentina	4	4.9	−47	293	−85	197	170	133
West Maranhao Basalts, Maranhao Basin, Brazil	3	9.3	−6.4	312.6	−85.3	262.5	175	1431
Anari and Tapirapua Formations, Western Brazil	5	3.8	−13.5	301	−65.5	250.3	196	3316
Bolivar Dykes, Venezuela	4	4.9	7.5	296.8	−66.9	245.6	202	150
Dolerite Dykes, Suriname	4	10	4	305	−82	320	232	701
Amana Formation, Paganzo Group, Argentina	4	7	−30.3	292.3	−83	317	240	1132
Mendoza Lavas, South Nihuil, Argentina	3	4	−33	292	−81	282	243	560
Sierra de la Ventana Redbeds, Argentina	3	14	−38	298	−78	219	250	560
La Colina Formation, Argentina	3	3.1	−30	292.7	−74	313	267	166
La Colina Formation, Argentina	3	3.3	−30	292.7	−81	327	267	166
Middle Paganzo II, Lower Beds, Argentina	3	2.5	−29.5	293	−59.5	357.5	273	620
Lowest Middle Paganzo, Argentina	4	4	−30	292	−66	326	273	283
South America (Fig. 3d)								
La Colina Formation, Paganzo Group, Argentina	3	3	−30.3	292.3	−78	249	278	1132
La Tabla Formation, Chile	4	5.7	−24.5	290.7	−51	347	284	1420
La Colina Basalt, Argentina	3	5	−30.1	292.6	−66	348	300	178
Pular and Cas Formations, Chile	6	9.6	−24.4	291.5	−57	350	306	1420
La Colina Formation, Argentina	6	0	−30	293	−49	343	306	1144
Itarare Subgroup, Tubarao Group, Brazil	3	11.2	−21.5	312.8	−57	357	306	798
Tepuel Group, Western Patagonia, Argentina	6	8.5	−43.5	289.6	−31.7	316.1	318	2805
Cratonic Australia (Fig. 3g)								
Bunbury Basalt, Western Australia	5	6.4	−33.4	115.6	−49	161	97	781
Mount Eclipse Sandstone, Northern Territory	6	8.6	−22.6	132	−37.6	52.6	344	2866
Brewer Conglomerate, Northern Territory	6	6	−23.9	133.7	−47.1	41	365	2726
Canning Basin Reef Complexes, W. Australia	6	15.2	−18	125.5	−62	23.2	368	2942
Reef Complex, Canning Basin, W. Australia	6	7.8	−18.3	125.6	−49.1	38	370	1345
Hermansburg Sandstone, Northern Territory	3	21	−24	133	−61	0.9	374	2574
Parke Siltstone, Northern Territory	5	14.9	−23.6	132.1	−60.9	318.1	384	2574
Tumblagooda Sandstone, Carnarvon Basin	5	3	−27.8	114.2	−26.7	33.7	465*	206
Jinduckin Formation, Northern Territory	4	13	−14.1	131.7	−13	25	482	202
Black Hill Norite, South Australia	3	3.8	−34.5	139.4	−37.5	34.4	487	2971
Chatswood Limestone and Ninmaroo Formation	6	7.4	−22.6	140.3	3.1	54.1	492#	3082
Giles Creek, Ross River, Amadeus Basin	3	10.4	−23.6	134.5	−38.3	24.5	505	1769
Lake Frome Group Combined, Flinders Ranges	3	10.1	−31.2	138.9	−31.4	26.9	505	1769
Billy Creek, Aroona Creek and Wirrealpa	6	14.4	−31.1	138.7	−37.4	20.1	515	1769
Lower Cambrian sediments, Kangaroo Island	3	12.3	−35.6	137.6	−33.8	15.1	518	1769
Pertaoorta Group, Amadeus Basin	6	7.3	−24.1	132.3	−32.7	11.5	525	1769
Hawker Group, Flinders Ranges, S. Australia	5	11.4	−31.2	138.6	−21.3	14.9	525	1769
Todd River Dolomite, Northern Territory	7	6.7	−23.4	133.4	−43.2	339.9	535	1070
Upper Arumbera Sandstone, Northern Territory	6	4.1	−23.4	133.4	−46.6	337.3	535	1070
Lower Arumbera and Upper Pertataka	6	12	−23.4	133.4	−44.3	341.9	550	1070
Brachina Formation, Adelaide Geosyncline	6	16	−30.5	139	−33	328	550	1648

*Poor age control; #suggested rotated by McElhinny *et al.* (2002) and excluded in APW spline path generation.

Continent, formation, country	Q	α_{95}	Location Lat.	Location Long.	Pole Lat.	Pole Long.	Age	Ref. no
East Antarctica (Fig. 3h)								
Lavas and dykes, Vestfjella	5	4.4	−73.7	345.1	−51.4	203.4	164	1548
Ferrar dolerites, N.Prince Albert Mountains	4	3.4	−74.5	162	−47.8	225.5	176	2721
Ferrar Dolerite Sill, Mt Cerberus, Dry Valleys	3	3.3	−77.4	161.8	−57.8	224.3	176	1838
Ferrar dolerites, Wright Valley	5	2.4	−77.5	161.6	−45.3	208	176	1599
Ferrar Dolerite, McMurdo Sound	5	10.2	−77.2	160	−50.5	211.4	176	1657
Storm Peak Lavas, Queen Alexandra Range	4	6.9	−84	165	−44.1	231.5	193	808
Vestfjella lavas and dykes	5	3.8	−73.3	345	−41.8	226.5	195	1154
Vanda lamprophyre and porphyry, Wright Valley	5	5.2	−77.5	161.6	−2.5	23.8	471	1599
South Victoria Land Intrusives	5	7.6	−77.5	162.5	−3.5	22.7	475	2966
Teall Nunatak, Victoria Land	5	7.2	−74.9	162.8	−11	21	479	3187
Lamprophyre Dykes, Taylor Valley	4	10.9	−77.6	163.4	−9.3	26.7	484	1079

Table 1. (*Continued.*)

Continent, formation, country	Q	α_{95}	Location		Pole		Age	Ref. no
			Lat.	Long.	Lat.	Long.		
Killer Ridge/Mt. Lok	4	12	−77.5	162.4	−7	21.4	499	#6
Granitic rocks, Wright Valley	4	8.1	−77.5	161.6	−5.4	18.5	500	1599
Sør Rondane Intrusives, Queen Maud Land	3	4.5	−72	24	−28.5	9.5	515	546

Q = Van der Voo (1993) classification factor (7 is the best score); α_{95} = 95 per cent confidence circle (* = A95 confidence circle); Lat./Long. = Location or palaeomagnetic pole latitude/longitude; age in million years.

Ref. no = global palaeomagnetic data base reference number (McElhinny & Lock 1996).

Additional references (not in global data base): #1 Derder *et al.* (2001) #2 Storetvedt *et al.* (1992) #3 Rakotosolofo *et al.* (1999) #4 Meert *et al.* (2001) #5 Torsvik *et al.* (2001) #6 Grunow & Encarnación (2000).

Supergroup). Madagascar (together with Seychelles and Greater India) rifted off Africa during the Jurassic, but seafloor spreading terminated in the Early Cretaceous (Coffin & Rabinowitz 1988), and Madagascar then became part of the African plate again. The Late Cretaceous of Madagascar is characterized by widespread magmatism, related to separation of Madagascar and India–Seychelles (Storey *et al.* 1995; Torsvik *et al.* 1998, 2000).

We use 12 poles from Madagascar (Fig. 3d). Most poles are Late Cretaceous, in addition to three Late Carbonif–erous–Triassic poles (Karoo Supergroup) and one Cambrian pole. A Late Carboniferous pole (305 Ma) differs from Late Permian (250 Ma) and Late Triassic (206 Ma) poles. The latter poles differ only slightly from Late Cretaceous poles that are the most reliable and best-dated poles from Madagascar.

2.3 Greater India

The Madagascar–Seychelles–Greater India trio rifted off East Africa during the Mid-Jurassic and, while seafloor spreading in the Mozambique Ocean terminated in the Early Cretaceous, East Antarctica (along with Australia) rifted off Greater India. Greater India–Seychelles rifted off the east coast of Madagascar at around 85 Ma. Greater India separated from the Seychelles at *c.* 65 Ma (Deccan Traps) and collided with Asia at around 50 Ma. During separation from the Seychelles, Greater India attained velocities of up to 18 cm yr^{-1}. This is the highest velocity recorded for any continental plate in Mesozoic and Cenozoic times, probably propelled by the Reunion hotspot (thermal buoyancy) and subduction of old and dense Tethyan oceanic lithosphere beneath Asia.

2.3.1 India

Twenty-five poles have been included from India (Fig. 3e). The selection can be divided into five groups: (1) nine K–T boundary poles (Deccan Traps related), (2) three Late Cretaceous poles, (3) five Early Cretaceous poles from the Rajmahal Traps, (4) five Permian to Early Jurassic sedimentary poles and finally (5) three poles of supposed Early Cambrian or possibly Late Precambrian age (red beds and evaporites). Groups 1–3 are considered to be the most reliable poles.

2.3.2 Pakistan

Data selection from Pakistan includes three Cambrian and two Permian poles. All poles plot near similarly aged poles from India, but suggested structural corrections (Klootwijk 1996) to the Pakistan poles owing to oroclinal bending in the Himalayas make them perhaps less reliable than the Indian poles. Regardless of this, inclusion/exclusion of a oroclinal bending correction for the Pakistan poles produces little change in the APW path analysis below. It is worth pointing out, however, that the age of Cambrian or possible Vendian sediments from India (no fossils—unconformably overlying the *c.* 750 Ma Malani Igneous Suite; Torsvik *et al.* 2001b) was originally deduced from a palaeomagnetic comparison with the better-dated Pakistan sediments (e.g. Athavale *et al.* 1972). If we correct the Pakistan poles as suggested by Klootwijk (1996), the dispersion of Pakistan–Indian poles increases markedly, perhaps making the original age assignment somewhat tenuous.

2.4 South America

We have included 35 poles of Carboniferous and younger age from South America. Most poles are from Argentina and Brazil and we exclude poles from areas suspected of rotations and/or translations. South America rifted off Africa at around 130 Ma, and many poles are derived from rocks that are coincident with breakup.

2.5 Cratonic Australia

The Australia collection includes 21 poles, all Vendian through Palaeozoic except one Late Cretaceous pole. Our Palaeozoic selection is quite similar to that of McElhinny *et al.* (2002) but we only include poles from Cratonic Australia, and exclude all poles within the Tasmian Fold-belt or east of the Tasmian Line. Owing to the lack of good Mid-Ordovician poles from Gondwana, the Tumblagooda Sandstone is critical, but
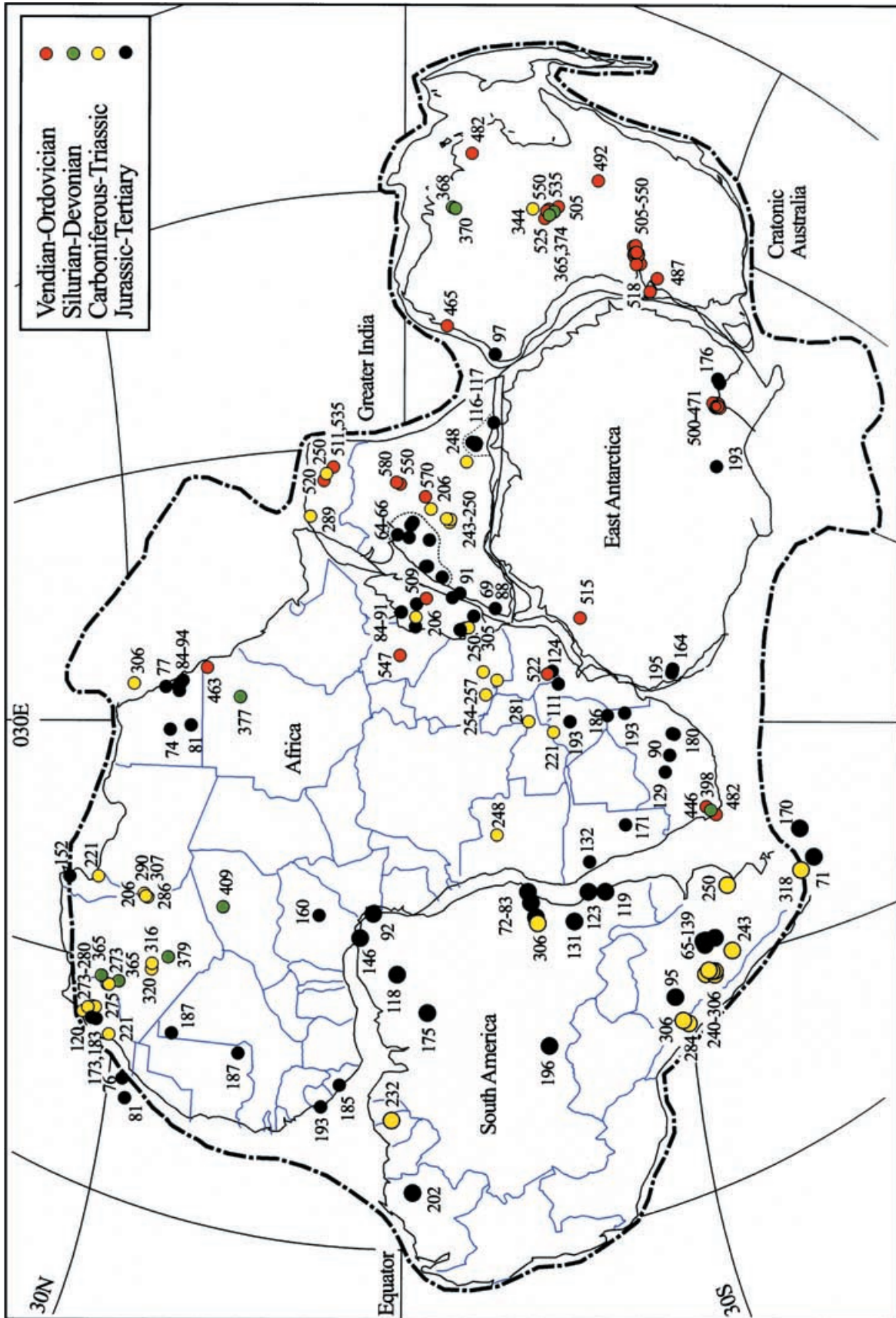
Figure 1. Geographic study location of palaeomagnetic poles (Table 1) for Gondwana. Africa is held fixed and relative fits are those of Lottes & Rowley (1990). Numbers are paleopole ages in Ma.
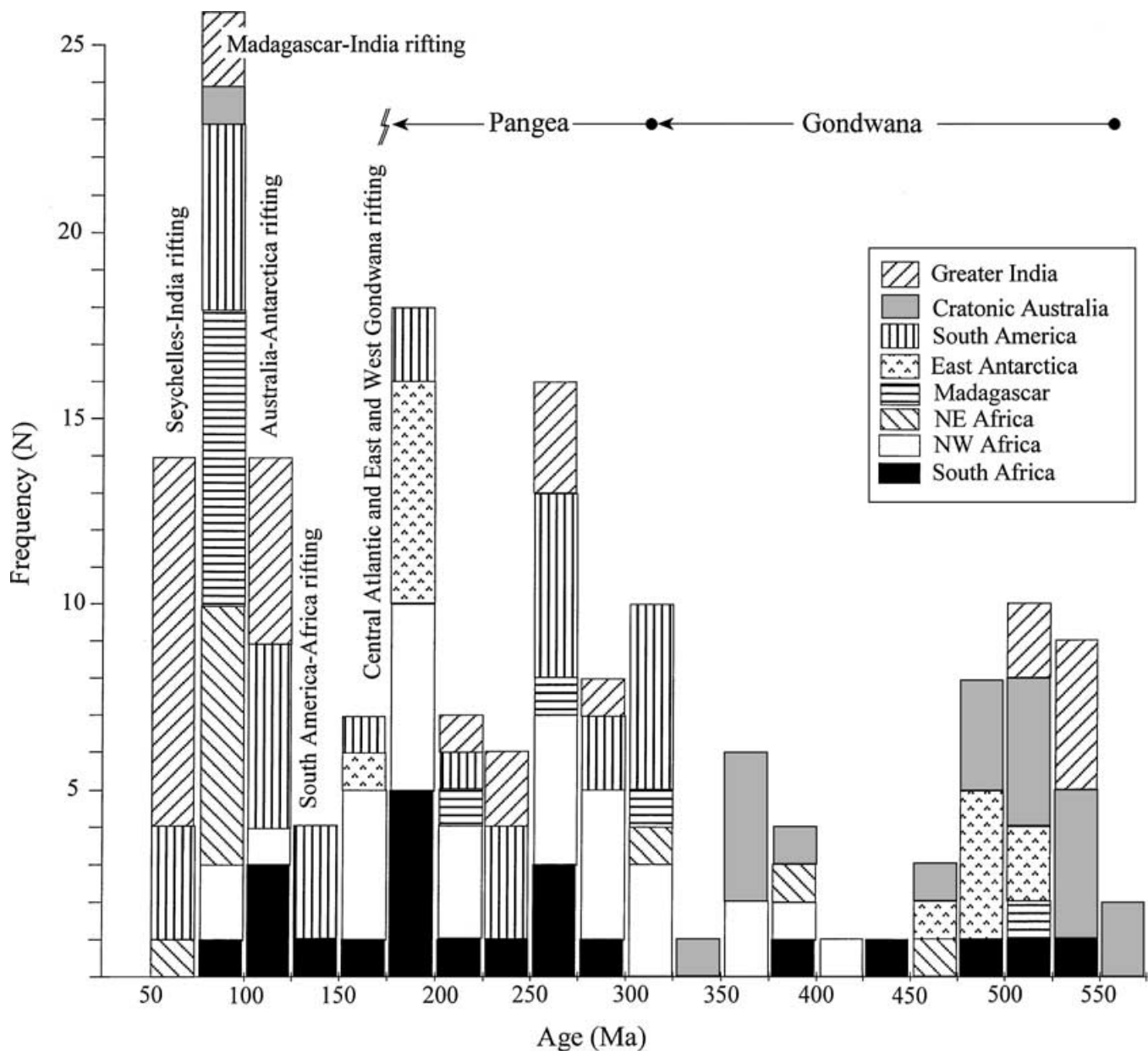
Figure 2. Frequency age-histogram for palaeomagnetic poles from Gondwana (Table 1). We have indicated the timing of some major events such as Gondwana–Pangea formation and Pangea breakup related events.

the age of this sandstone (assigned a numerical mean age of 465 Ma by McElhinny *et al.* 2002) is not very well constrained. The *c.* 492 Ma Chatswood Ninmaroo Fm pole is somewhat anomalous when compared with other Late Cambrian–Early Ordovician poles, and McElhinny *et al.* (2002) suggest a possible tectonic rotation (study area is located close to the Tasmian Line).

2.6 East Antarctica

Our selection includes 14 poles, mainly Early Ordovician and Jurassic poles in addition to one Middle Cambrian pole. East Antarctica together with Australia rifted off Greater India (and Madagascar–Seychelles) during the Early Cretaceous, whilst significant separation of East Antarctica from Australia did not take place until the Late Cretaceous–Early Tertiary.

3 A REFINED GONDWANA APW PATH

Numerous APW paths have been proposed for Gondwana and we show examples (Fig. 4) of three recent APW paths (Smith 1999; Grunow 1999; McElhinny *et al.* 2002), along with a South Pole path constructed purely from climatological–sedimentological indices (Scotese & Barrett 1990). Gondwana fits used to construct the different APW paths differ somewhat but this cannot explain the very different paths.

Table 2. Gondwana reconstruction fits used in this paper (relative South Africa).

Age	Lat	Long	Ang	Lat	Long	Ang	Lat	Long	Ang	Lat	Long	Ang	Lat	Long	Ang	Lat	Long	Ang	Lat	Long	Ang
	Madagascar			India			South America			Australia			East Antarctica			NW Africa			NE Africa		
10				23.5	33.5	−4.6	59.4	321.5	3.7	11.7	49.5	−6.5	8.6	310.6	1.5						
20				29	24.8	−7.3	57.9	323	7.5	14.5	46.7	−11.8	10.8	312	2.8						
30				24.9	34.2	−12.2	57.1	325.2	11.6	13.8	48.3	−16.8	14.7	310	4.6						
40				22.7	41.9	−16.8	57.1	327	15.4	15.1	49.3	−21.7	15.2	313	6.5						
50				23.7	35.9	−22.1	58.9	328.3	19.5	15.9	52.5	−23.7	10.3	317.1	8.8						
60				23.2	26.9	−29.8	61.5	328.2	23	15.1	57.8	−24.4	4.4	320.4	10.6						
70				20.9	18.8	−43.2	63.3	326.4	26	11.5	60.3	−25.5	0.5	318.5	12.2						
80				23.9	16.8	−48.8	62.9	325.8	31	16.3	69.4	−27.1	−4.6	320.3	16						
90				22.5	23.6	−53	59.1	325.6	36.8	15.8	82.3	−28.9	−4.1	326.4	22.1						
100				21.4	30.7	−56.8	55.9	325.3	42.3	17.9	95	−31.8	−5.6	331	29.3	0	0	0	0	0	0
110				21.4	30.7	−56.8	53.4	325.1	48	20.5	106.2	−35.3	−6.5	333.9	36.6	3.1	1.9	2.6	22.7	252.3	−0.8
120	3.5	283.4	1.6	21.9	32.2	−57.4	51.4	325.3	53.1	23.3	115	−39.5	−7.7	336	43.9	6.2	3.8	5.2	20.2	236.7	−1.7
130	3.4	280.8	6.9	22.3	36.9	−61	50.1	327.2	54.9	28.2	123	−43.4	−11.9	339	50.4	9.3	5.7	7.8	16.3	221.7	−2.5
140	5.1	283.3	8.1	22.6	38.1	−61.1	49.8	327.4	55	23.1	119.1	−46	−7.8	334.1	50.6	9.3	5.7	7.8	16.3	221.7	−2.5
150	4	288.6	11.3	24	41.4	−61.5	49.6	327.5	55.1	19.4	118.4	−49.2	−4.7	331	52.8	9.3	5.7	7.8	16.3	221.7	−2.5
160	−0.9	281.7	16.9	25.6	45.1	−66	49.3	327.7	55.2	21.6	118.9	−52.9	−6.8	329.4	56.3	9.3	5.7	7.8	16.3	221.7	−2.5
170	−3.4	278.3	19.7	26.4	46.9	−68.3	49	328	55.2	22.7	119.2	−54.8	−7.7	328.6	58	9.3	5.7	7.8	16.3	221.7	−2.5
180	−3.4	278.3	19.7	26.4	46.9	−68.3	48.7	328.2	55.3	22.7	119.2	−54.8	−7.7	328.6	58	9.3	5.7	7.8	16.3	221.7	−2.5
190	−3.4	278.3	19.7	26.4	46.9	−68.3	48.5	328.4	55.4	22.7	119.2	−54.8	−7.7	328.6	58	9.3	5.7	7.8	16.3	221.7	−2.5
200	−3.4	278.3	19.7	26.4	46.9	−68.3	48.2	328.6	55.5	22.7	119.2	−54.8	−7.7	328.6	58	9.3	5.7	7.8	16.3	221.7	−2.5
210	−3.4	278.3	19.7	26.4	46.9	−68.3	47.9	328.7	55.6	22.7	119.2	−54.8	−7.7	328.6	58	9.3	5.7	7.8	16.3	221.7	−2.5
220	−3.4	278.3	19.7	26.4	46.9	−68.3	47.6	328.9	55.7	22.7	119.2	−54.8	−7.7	328.6	58	9.3	5.7	7.8	16.3	221.7	−2.5
230	−3.4	278.3	19.7	26.4	46.9	−68.3	47.4	329.1	55.7	22.7	119.2	−54.8	−7.7	328.6	58	9.3	5.7	7.8	16.3	221.7	−2.5
240	−3.4	278.3	19.7	26.4	46.9	−68.3	47.1	329.3	55.8	22.7	119.2	−54.8	−7.7	328.6	58	9.3	5.7	7.8	16.3	221.7	−2.5
+250	−3.4	278.3	19.7	26.4	46.9	−68.3	46.8	329.5	55.9	22.7	119.2	−54.8	−7.7	328.6	58	9.3	5.7	7.8	16.3	221.7	−2.5

The APW paths shown in Fig. 4 differ substantially and may appear chaotic, but they do have two common features: (1) Mid-Late Cambrian to Ordovician poles are centred in NW Africa and (2) Permian and Early Mesozoic mean poles are grossly similar. The Silurian and Devonian sections, however, are very different. For example the end-member path of McElhinny *et al.* (2002) shows a Siluro-Devonian counterclockwise loop followed by a Devono-Carboniferous clockwise loop, whilst the other paths show a much smoother transition from Ordovician to Permian times. Other complex loop paths published in the literature are those of Kent & Van der Voo (1990) and Bachtadse & Briden (1990). *Data selection is the prime factor influencing the differences in the APW paths*, and Gondwana fits are of secondary importance.

Based on the reconstruction parameters listed in Table 2 (but interpolated to 1 Ma when rotating poles to a common reference scheme) we have produced a new APW path for Gondwana, not only for Vendian (when Gondwana was assembled) to Jurassic times (when core Gondwana/Pangea broke apart), but as young as the Cretaceous–Tertiary boundary using magnetic anomaly fits.

Fig. 5 shows two versions of our new Gondwana path; one is a spherical spline path (Fig. 5a) adopting a moderately high smoothing parameter (=1000 and *Q*-factor weighting; see the procedure in Torsvik *et al.* 1996) in order to smooth out some of the complexity in the data set. The Vendian to Early Ordovician part of the path is well constrained but the quality dwindles through the Mid-Palaeozoic, as is true for all previously published APW paths for Gondwana (see the discussion in Van der Voo 1993). The Cambrian section shows some similarities with that of Meert *et al.* (2001), whilst the South Polar movement across Gondwana during the Ordovician–Silurian is comparable to that suggested from climatic sensitive lithologies (Scotese & Barrett 1990). Compared with some previous APW paths, ours is somewhat more complex, but the counterclockwise Siluro-Devonian and clockwise Devono-Carboniferous loops show gross similarities with those of Kent & Van der Voo (1990) and McElhinny *et al.* (2002). These loops very much hinge on Devonian poles from Australia and the 409 Ma Air pole from NW Africa.

In Fig. 5(b) we show a path using running mean poles (20 Ma window, 10 Ma interval). This path is grossly similar to the spherical spline path (Fig. 5a) and we have indicated when the mean poles are relatively well determined ($N \geq 3$, $\alpha_{95} < 20$) compared with those estimates with low N or large α_{95}.

Based on the spherical spline path (Fig. 5a) we have calculated the latitudinal change, drift rates (minimum, only latitudinal) and rotation for a specific location in Africa (0°, 030°E). Drift rates peak at 10–12 cm yr^{-1} in the Cambrian and Permo-Carboniferous, but typically are below 8 cm yr^{-1} throughout the Phanerozoic, hence our APW path for Gondwana suggests mean velocities that are comparable with modern plate tectonic velocities. Gondwana rotations are typically below 2° Ma^{-1} except during an apparent Mid-Carboniferous high (16° Ma^{-1}). This high value, however, is a pure artefact because our reference location was located at the South Pole at this time. Late Cambrian through to Early Devonian palaeogeographic implications of the revised Gondwana APW path are discussed in Cocks & Torsvik (2002), whilst the Carboniferous and younger geological history is evaluated below.
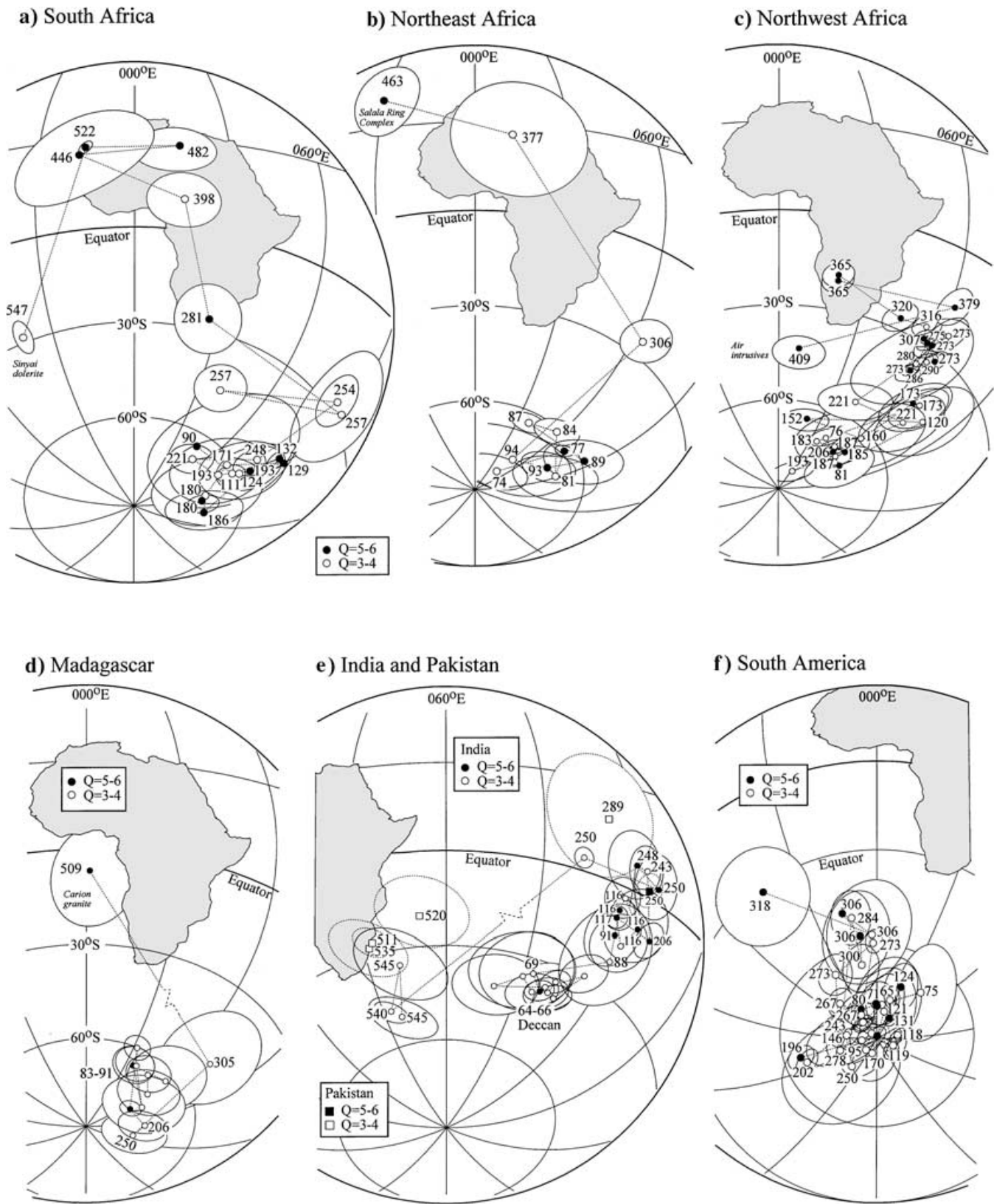
Figure 3. Palaeomagnetic poles with confidence ovals for Gondwana elements. Numbers are paleopole ages in Ma. All poles are *south* poles and are listed in Table 1. *Q* is the quality factor (Van der Voo 1993).
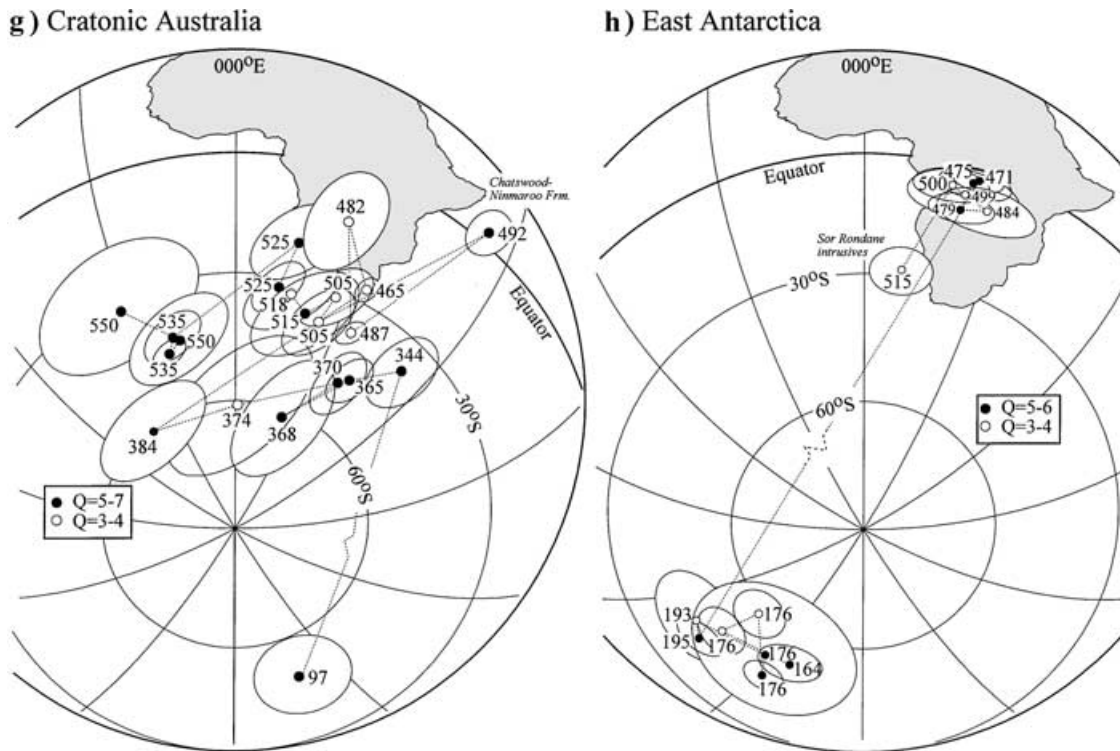
Figure 3. (*Continued.*)

4 COMPARISON OF GONDWANA AND LAURUSSIA

Fig. 7 compares running mean poles from Laurussia (North America and Europe; Torsvik *et al.* 2001c; mean poles >300 Ma based on data listed in Torsvik *et al.* 1996) with those from our new Gondwana path, using the reconstruction parameters of Table 5, whilst Fig. 8 shows the great circle distance (GCD in degrees) between mean poles of the same age as a function of geological time. Mean poles in Fig. 7(a) were calculated in the normal fashion assuming a GAD field, and to keep our diagram simple we compare mean poles in 20 Ma intervals (also the time window length) from 350 to 70 Ma. Figs 7(b)–(f) show a comparison of mean poles with steadily increasing octupole contributions (5 per cent intervals). Individual poles were recalculated with octupole contributions (Appendix A); we then calculated new running mean paths for Gondwana and Laurussia, and the Gondwana APW path was subsequently rotated into the Laurussia frame (Table 2) in the process. We rotated the Gondwana poles to NW African coordinates (Lottes & Rowley 1990), then used the rotation parameters of Müller *et al.* (1997) for fitting NW Africa to North America (175–70 Ma); we have used a *c.*4° tighter fit for the Permo-Triassic in order to account for some pre-drift (Mid-Jurassic) extension in the Central Atlantic (Table 5). This tighter fit also produces an improved fit between palaeomagnetic poles from Laurussia and Gondwana. Note that all poles in Fig. 7 are plotted as north poles as compared with south poles in Fig. 3.

For poles calculated with a GAD field model we note that the Late Cretaceous and Jurassic APW sections show a reasonable, but not a perfect match (the Gondwana path has somewhat higher pole latitudes), whilst the Triassic and older sections differ substantially. In plate tectonic terms, Fig. 7(a) indicates that with a GAD field model, a Pangea-A type fit is possible for the Jurassic (Fig. 9, 170 Ma GAD), but not for older times. The 350 Ma mean poles differ substantially in all comparisons because the continental amalgamation into Pangea was only at its initial stage at this time. In addition, 150 Ma mean poles always differ. The Gondwana 150 Ma mean pole, however, is based on only three poles and one pole (from Tunisia) differs substantially from the two other poles (Brazil and Nigeria).

From geological evidence, the bulk of Pangea was assembled by the Late Carboniferous, except for terranes and microcontinents in the Palaeo-Tethys realm that did not join Pangea until just prior to its breakup in the Mid-Jurassic. It is evident that Laurussia and Gondwana in our Late Carboniferous–Early Triassic reconstructions with the GAD model (e.g. 310 and 250 Ma in Fig. 9) cannot be reconciled with a classic Pangea-A fit (see also Van der Voo 1993; Van der Voo & Torsvik 2001) because Gondwana needs to be positioned in latitudes that are too far north relative to Laurussia. Many workers therefore have invoked different (Pangea-B type) reconstructions and subsequent large dextral transcurrent motions (e.g. Morel & Irving 1981; Muttoni *et al.* 1996; Torcq *et al.* 1997) in order to achieve the typical Pangea-A Jurassic fit that is universally considered as the starting point for Pangea breakup (Fig. 9) in the Mid-Jurassic (Van der Voo 1993). Conversely, Van der Voo & Torsvik (2001) suggested that the Pangea problem can be resolved by invoking non-dipole fields (octupoles) and below we explore this in significantly greater detail.

A comparison of Gondwana–Laurussia mean poles with steadily increasing octupole contributions (5 per cent intervals) reveals some remarkable features: (1) with G3 ≈ 0.05 the Cretaceous–Mid-Jurassic segment is clearly improved, (2) G3 ≈ 0.1 provides a best fit for the

Table 3. Smoothed APW spline path listed in approximately 10 Ma intervals for South Africa coordinates (see Fig. 5a).

Age	Plat	Plon	Plat	Plon
	GAD		G3 Optimized	
60	−71.95	48.93	−68.88	50.62
69	−68.92	53.95	−66.36	51.37
80	−68.8	57.26	−66.44	51.23
90	−69.35	67.42	−67.7	53.53
101	−67.26	82.05	−67.47	64.46
111	−60.79	84.49	−65.3	79.05
120	−53.86	82.31	−59.19	82.35
130	−50.08	79.09	−53.09	81.07
140	−52.52	72.06	−50.09	78.45
150	−56.86	65.3	−52.75	71.42
160	−57.2	71.83	−56.75	63.88
170	−56.61	80.62	−56.42	68.85
180	−62.65	83.87	−55.27	76.87
190	−68.92	77.59	−60.96	79.83
203	−67.83	64.03	−66.31	62.28
214	−61.08	62.11	−59.52	60.97
222	−57.07	64.1	−55.13	61.41
232	−53.01	68.98	−49.67	62.92
240	−50.47	72.57	−45.41	64.66
251	−45.98	73.89	−39.45	66.19
261	−39.49	69.1	−35.3	62.96
270	−33.55	62.05	−31.68	57.13
280	−29.74	54.85	−28.77	51.43
290	−28.71	55.1	−27.79	51.21
300	−27.61	54.52	−27.23	49.17
307	−25.65	50.71	−25.61	45.18
320	−17.89	38.82	−18.28	36.42
329	−8.47	32.98	−9	34.63
341	1.84	27.57	−0.72	34.03
353	1.2	23.31	1.85	29.27
361	−3.74	20.7	−1.29	24.68
370	−8.78	18.99	−6.22	21.04
380	−14.58	18.41	−12.79	17.21
391	−19.07	15.34	−17.98	12.73
400	−22.07	13.45	−20.16	11.44
409	−25.23	9.95	−20.76	9.57
419	−19.44	2.95	−15.94	5.15
429	−6.59	356.06	−6.25	0.39
439	8.57	351.75	5.6	357.52
450	21.81	352.25	16.16	358.37
459	28.68	357.36	25.49	2.93
470	32.85	3.37	30.99	5.04
481	32.26	6.79	30.18	6.14
489	29.27	7.08	26.52	7.35
500	24.08	4.28	22.55	6.86
510	17.24	0.64	16.1	4.91
521	12.25	354.56	12.39	356.39
531	1.87	344.93	3.77	341.38
540	−7.38	337.21	−4.39	332.57
550	−12.85	330.21	−8.51	324.06

Plat/Plon = pole latitude/longitude; GAD = geocentric axial dipole; G3 = octupole (see text).

Late Triassic–Mid-Jurassic and (3) G3 ≈ 0.15 leads to an almost perfect match in the Permo-Carboniferous segments (see Figs 7 and 8). This suggests that during the considered 310–70 Ma interval the non-dipole octupole field contribution is likely to have decreased with time. However, in detail, the GAD model nevertheless appears to show fluctuating GCD values of around 5°–15°. Improvement in the APW fits is seen when values fall below the GAD curve (heavy grey curve) with the lower diagram in Fig. 8 showing optimal values of G3. We notice that a G3 of 0.05 to 0.1 marginally improves the Cretaceous section (0.05 is best), whilst for Triassic and older times, significant G3 values are needed to improve the fits. The 130 Ma mean pole differs from all other mean poles because a GAD model is the best match (indeed a few

Table 4. Running mean APW path in South African coordinates (see Fig. 5b); age ±10 Ma.

Age	Plat	Plon	A95	N	LR
60	−67.95	56.75	4.34	11	33.94
70	−68.18	56.58	3.59	17	77.93
80	−68.56	57.47	3.5	22	77.93
90	−69.42	62.13	3.54	23	66.26
100	−70.97	72.96	6.95	7	62.66
110	−56.56	83.17	4.81	9	52.83
120	−54.44	81.4	4.21	14	62.58
130	−48.42	78.79	5	9	62.77
140	−50.47	75.57	9.75	4	36.52
150	−59.82	57.41	14.43	3	31.23
160	−60.25	73.56	15.77	4	79.95
170	−59.12	82.85	6.5	13	74.18
180	−61.75	79.6	5.64	16	74.18
190	−69.27	76.24	4.62	13	63.67
200	−69.03	67.67	5.88	10	61.84
210	−65.51	57.65	7.53	4	30.12
220	−54.3	61.54	23.81	3	49.61
230	−53	64.57	10.73	5	66.36
240	−49.51	72.79	5.71	6	36.55
250	−47.65	72.04	8.53	13	44.47
260	−47.13	69.14	11.26	10	44.47
270	−34.84	61.95	9.26	10	64.63
280	−30.04	59.54	7.35	14	64.63
290	−29.27	56.64	10.59	7	63.25
300	−27.89	57.21	5.84	8	61.89
310	−26.18	51.57	8.37	10	72.65
320	*−21.36*	*41.26*	*31.92*	*3*	*69.29*
330	*−21.54*	*48.58*	*0*	*1*	*0*
340	*11.85*	*27.65*	*0*	*1*	*0*
350	*11.85*	*27.65*	*0*	*1*	*0*
360	−8.92	18.23	11.24	5	48.02
370	−6.1	20.26	16.94	8	48.02
380	*−6.95*	*14.68*	*36.7*	*5*	*41.15*
390	*−10.69*	*0.49*	*180*	*2*	*17.51*
400	*−16.22*	*15.86*	*180*	*2*	*53.12*
410	*−42.44*	*17.01*	*0*	*1*	*0*
440	*25*	*343*	*0*	*1*	*0*
450	*25*	*343*	*0*	*1*	*0*
460	*32.1*	*351.38*	*100.25*	*2*	*27.29*
470	34.5	357.56	14.51	5	55.03
480	31.47	5.94	7.92	7	24.24
490	33.52	9.54	11.96	7	24.24
500	27.11	6.48	16.81	6	30.44
510	14.78	0.87	6.55	8	42.15
520	13.69	356.95	7.99	8	36.48
530	6.02	347.16	12.72	8	34.85
540	−8.24	336.79	9.11	9	33.53
550	−10.21	334.06	11.94	6	27.24

A95 = 95 per cent confidence circle around the mean poles; N = number of poles; LR = site latitude range for poles. Entries in italics are means based on N < 3 or A95 > 20°.

per cent *negative* G3 is the best match). Our analysis implies that it is only possible to have a Pangea-A type fit from 310 to 170 Ma (Fig. 9) if we assume that the APW misfits between Gondwana and Laurussia are caused by G3 contributions.

5 INTERNAL DISPERSION IN THE GONDWANA DATA SET

In the analysis above we use a 'tectonic' argument, namely that Pangea-A is preferable over other Pangea (B, C, D) fits to evaluate G3 contributions (in a similar fashion to Van der Voo & Torsvik 2001). Unfortunately, we cannot use the same analysis as Van der Voo & Torsvik (2001) with the slope of the line through predicted–observed pairs because Gondwana straddles the pole. This means that an analysis has to be based on the farsidedness of poles, as seen from the sampling site, and as G3 is increased in the analysis, the farsidedness should diminish.
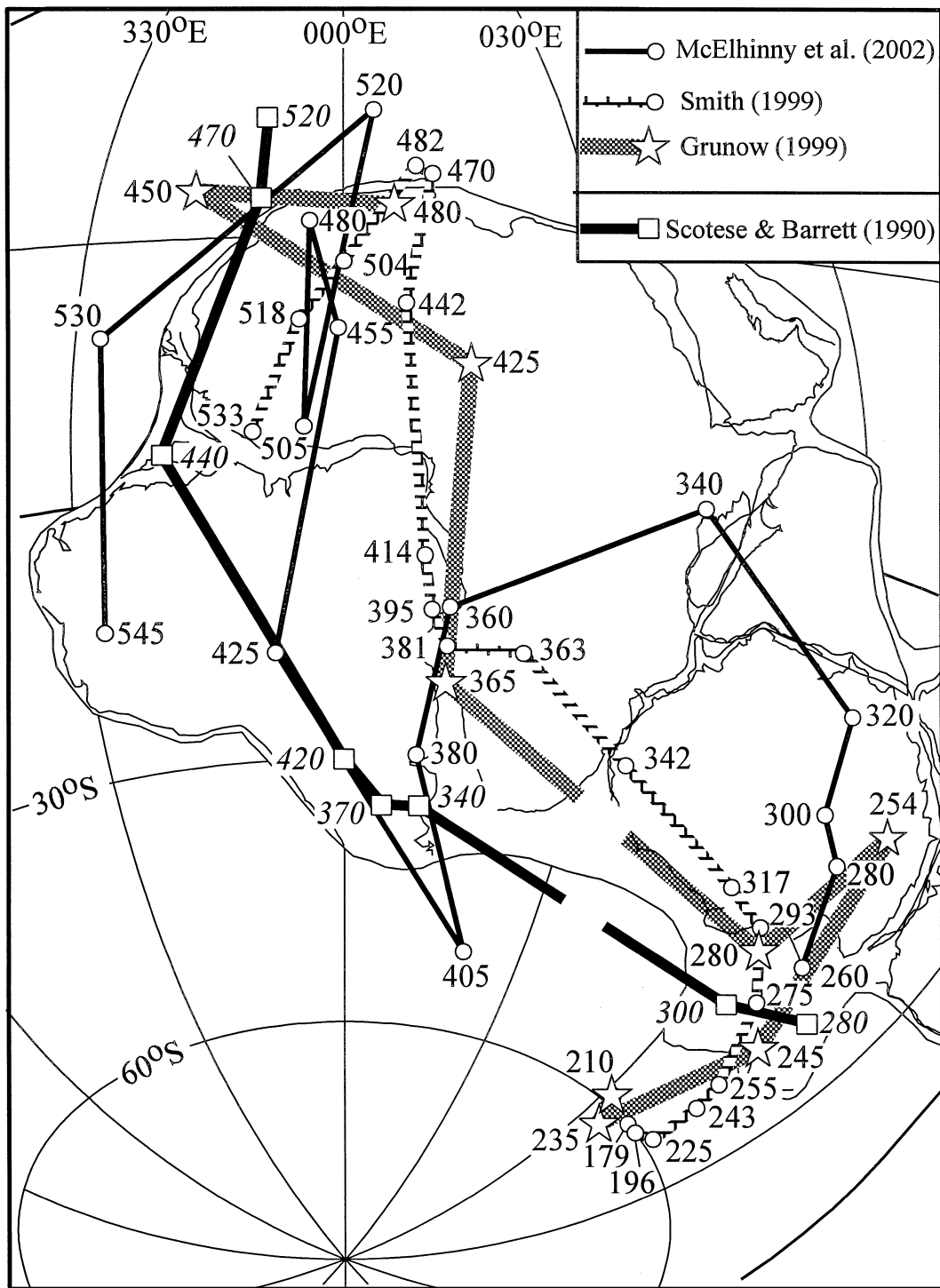
Figure 4. Examples of some previously published APW paths for Gondwana (Cambrian to Jurassic). Numbers are in millions of years.

However, incorporation of non-dipole fields is testable in other ways, because the precision parameter k should increase or the 95 per cent confidence circle around the mean pole (A95) should decrease as the G3 contribution is optimized. Recall that, for example G3 = 0.1 produces a maximum 'GAD offset' of 832 km at 53°north or south, whilst at the equator or the geographic poles, zonal octupole fields produce no errors.

Torsvik *et al.* (2001a) listed A95 for a GAD and a G3 = 0.08 model for Laurussia. Inspection of their Table 1 (40–130 Ma; 5 Ma intervals) shows that nine of the 19 listed mean poles actually show a minor increase in A95, but over the entire interval the statistical significance of these changes is low. This compilation included only data from North America and Europe with a limited spread in sampling latitudes.
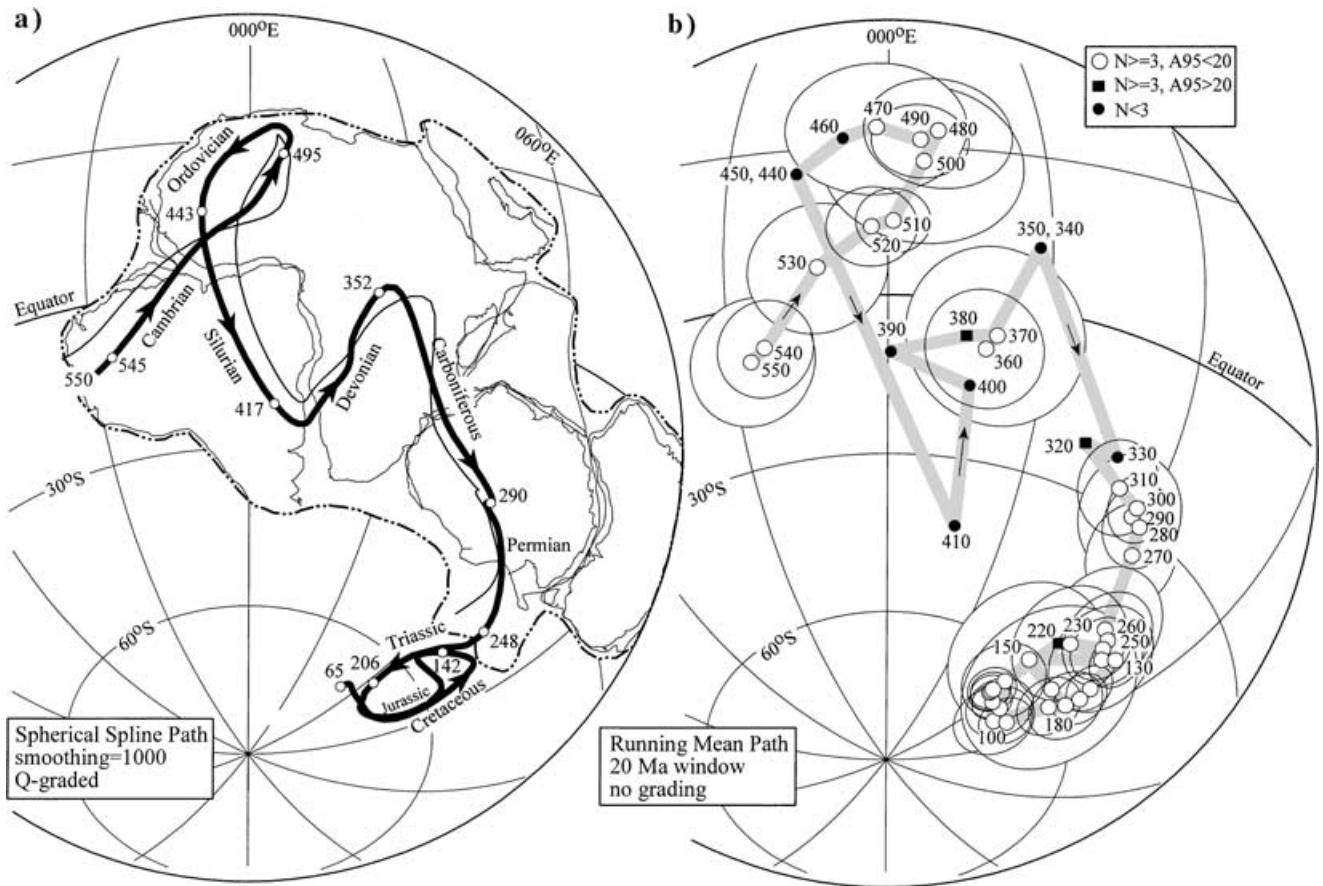
Figure 5. A spherical spline (a) and (b) a running mean (20 Ma window) APW path for Gondwana based on the present analysis. Mean poles in (b) are shown with A95 confidence circles. Euler parameters for Gondwana fits are listed in Table 2, whilst APW paths are listed in Tables 3 and 4. The thin solid line in (a) is a G3 optimized path (see text) and ends at 250 Ma for clarity.

Gondwana in Space and Time (Central Africa:0, 030°E)
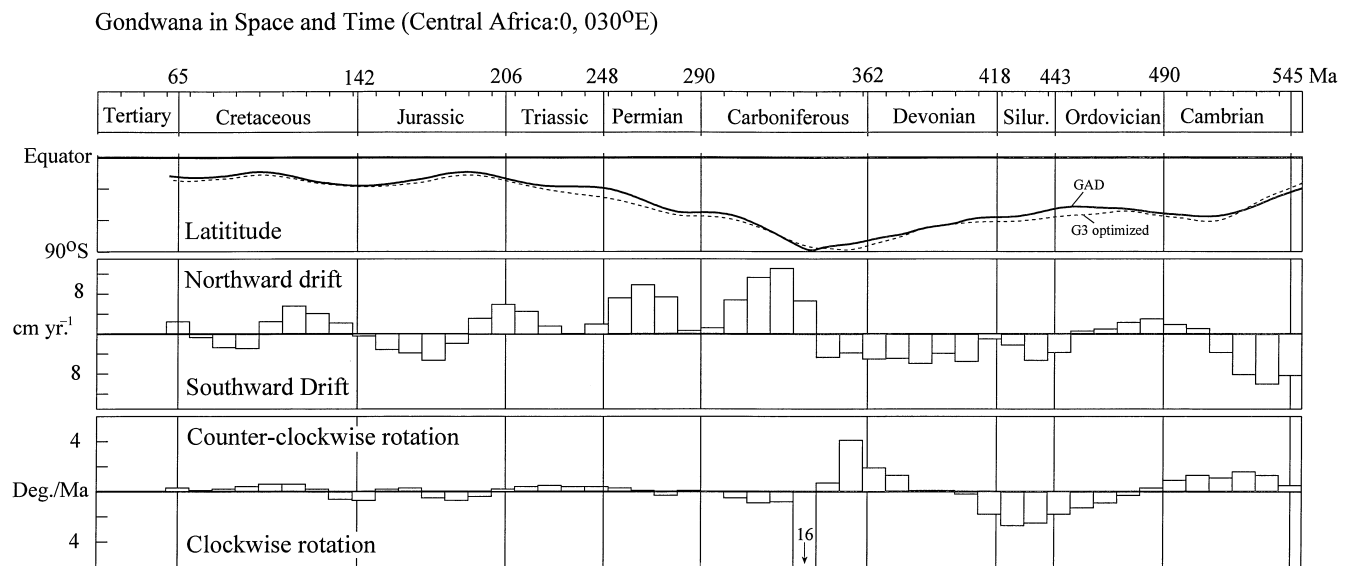
Figure 6. Latitude drift for a central African location (top), latitudinal drift rates and angular rotations (bottom) for 'Gondwana' based on the spherical spline path in Fig. 5(a). The stippled curve in the top diagram is based on a G3 optimized path (Table 3).
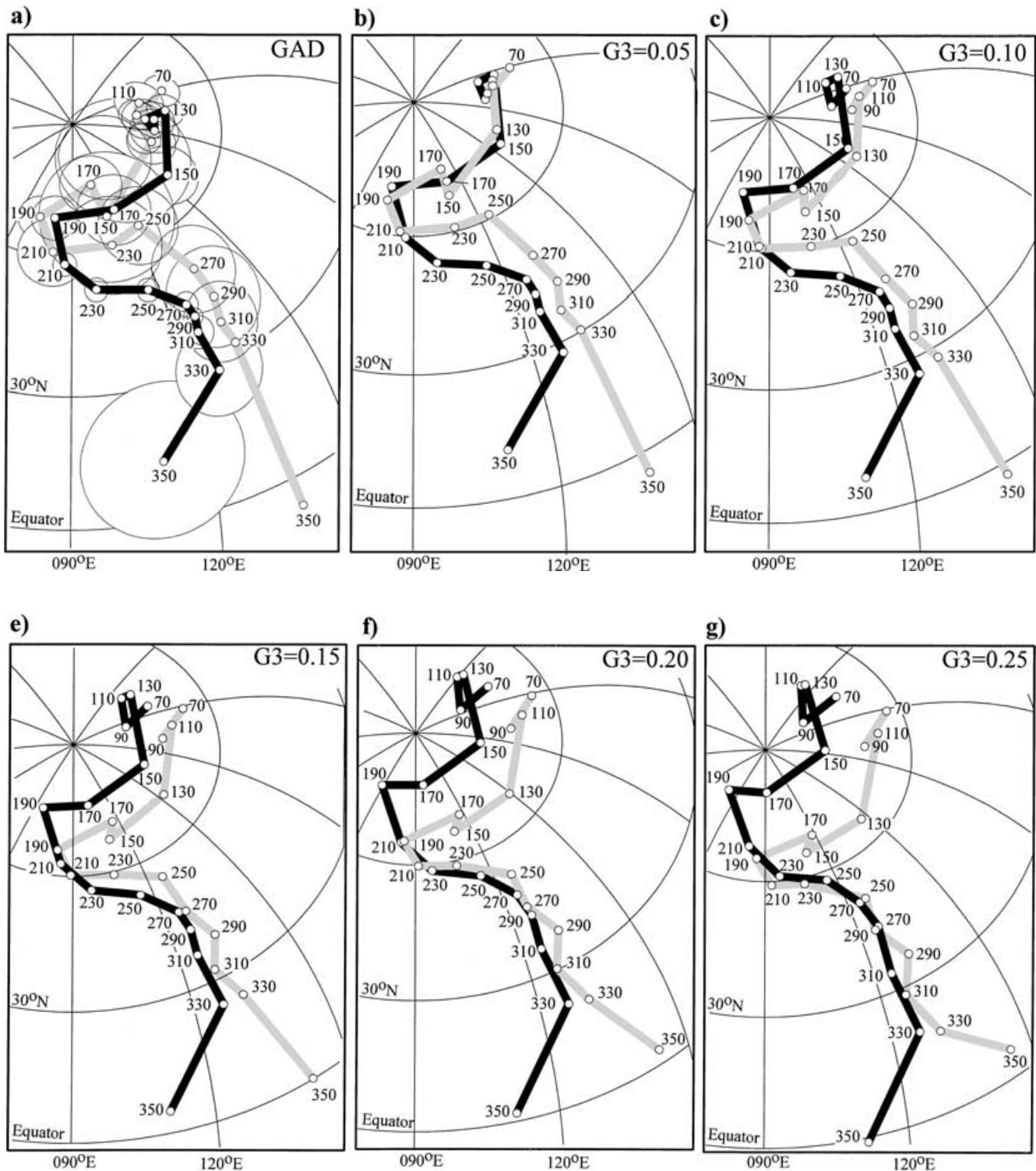
Figure 7. Comparison of Laurussia (black) and Gondwana (grey) running mean APW paths in a GAD field model (a) and with increasing G3 contributions in 0.05 intervals (b–g). Reconstruction parameters are given in Table 5.

Their Early Tertiary mean poles, for example, did not show any changes (see their 55 and 60 Ma entries). Including high-latitude sites in Greenland, however, dramatically reduces A95, illustrating that a wider range of site latitudes is needed to detect the effects of non-dipole fields.

In Fig. 10 we evaluate the change in A95 as a function of increasing G3 (0–0.15). We only show mean values where $N \geq 3$, A95 < 20 and sampling latitude spread $> 35°$. For more than half of the considered time intervals, A95 is reduced (eight out of 14) with various values

Table 5. NW Africa to North America fits.

Age	Lat	Long	Angle
10	80.1	50.8	−2.5
20	79.55	36.26	−5.45
30	77.25	10.2	−8.48
40	75.38	359.31	−11.89
50	75.53	356.23	−15.45
60	80.27	0.2	−18.66
70	82.05	355.8	−22.06
80	78.73	342.56	−26.52
90	74.74	339.5	−33.95
100	71.73	339.77	−41.2
110	68.71	339.97	−48.45
120	66.26	340.33	−54.79
130	65.98	341.41	−57.22
140	66.09	341.59	−59.55
150	66.59	342.19	−62.32
160	67.12	344.74	−66.62
170	67.02	346.83	−72.1
180	66.96	347.98	−75.98
190	66.97	347.99	−76.84
200	66.98	347.99	−77.71
210+	66.99	348	−78.57
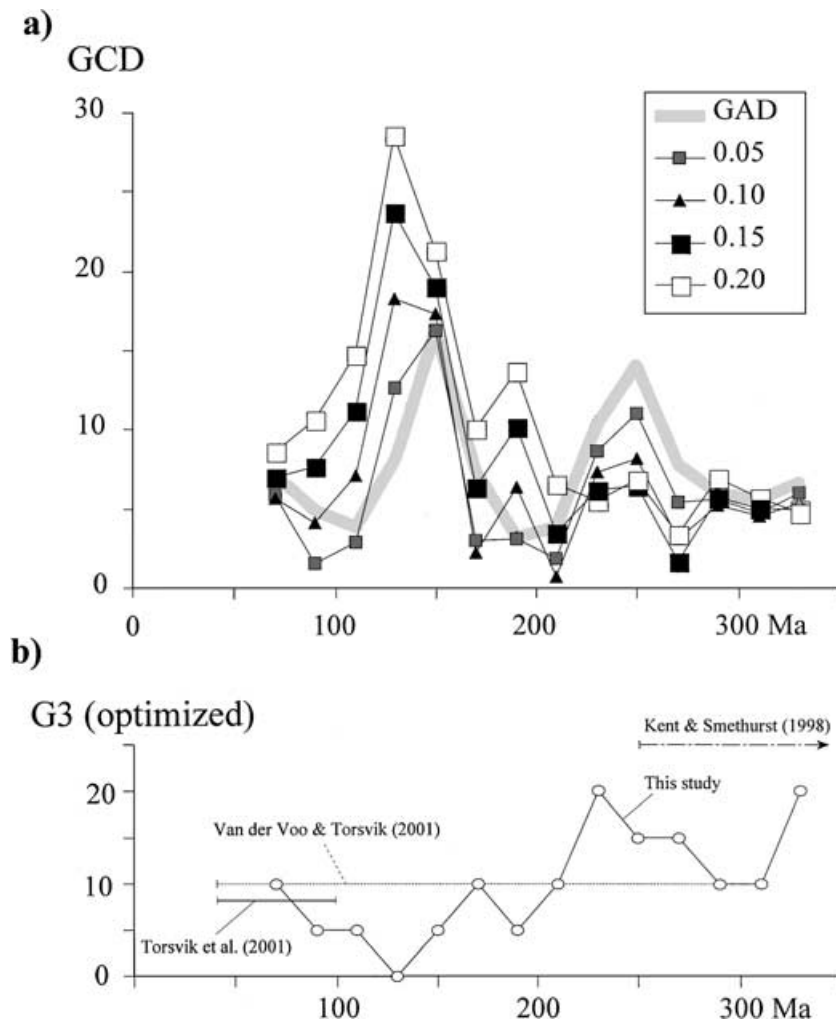
Figure 8. (a) Variation in great circle distance (GCD) between Laurussia and Gondwana mean poles in Fig. 7 with GAD and G3 models. The lower diagram (b) shows the optimized G3 value that minimizes GCD in the top diagram.
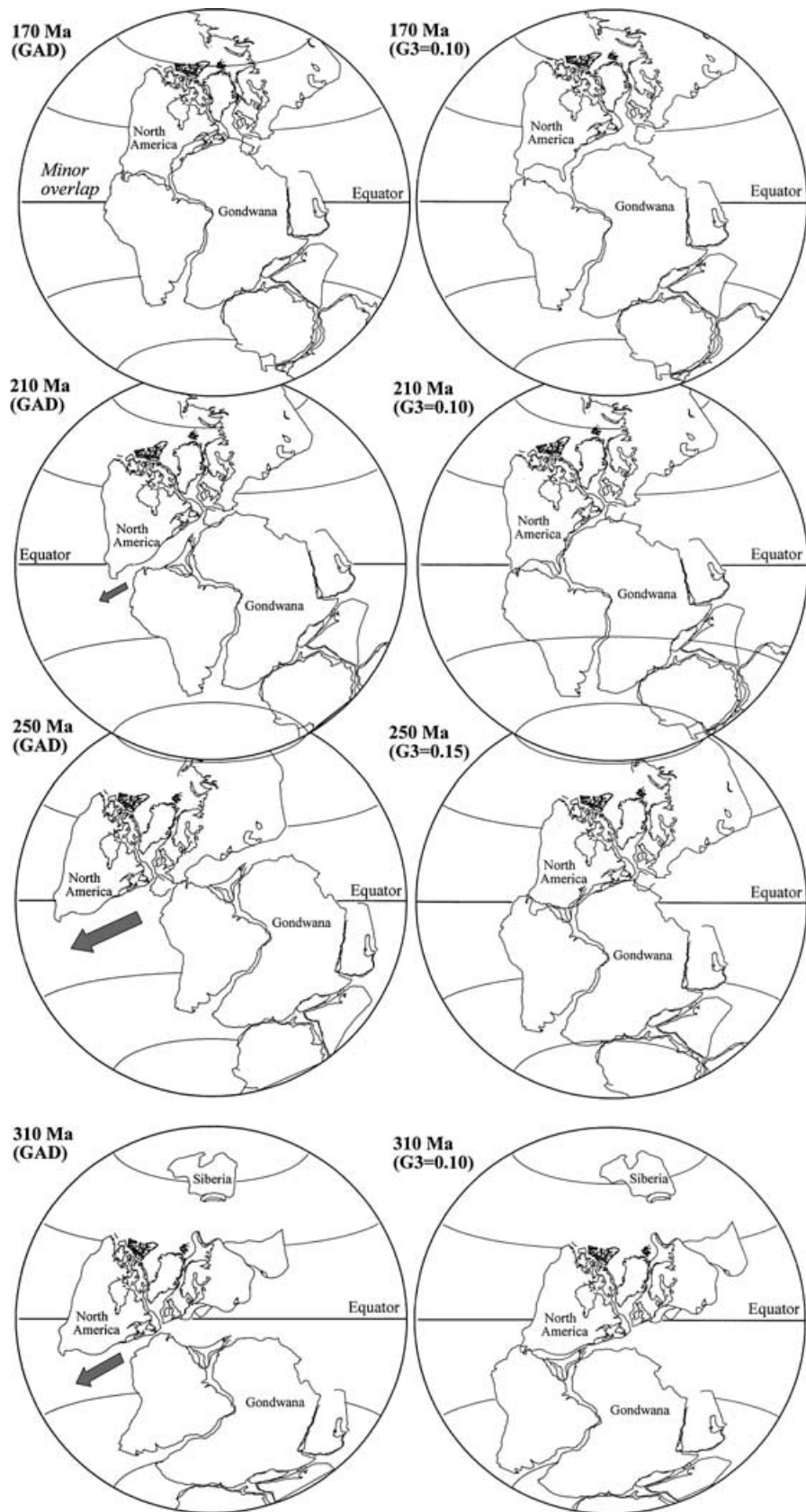
Figure 9. Examples of Pangea reconstructions based on GAD models (left) and G3 contributions. Note that only the 170 Ma reconstruction shows a Pangea-A type configuration. The 210 Ma reconstruction shows a minor misfit, but all other GAD reconstructions cause substantial overlap between Laurussia and Gondwana. Hence, Gondwana is moved sideways and the large arrows show that Gondwana must be displaced dextrally to achieve a Pangea-A fit. The right-hand side diagrams rectify most of this overlap.
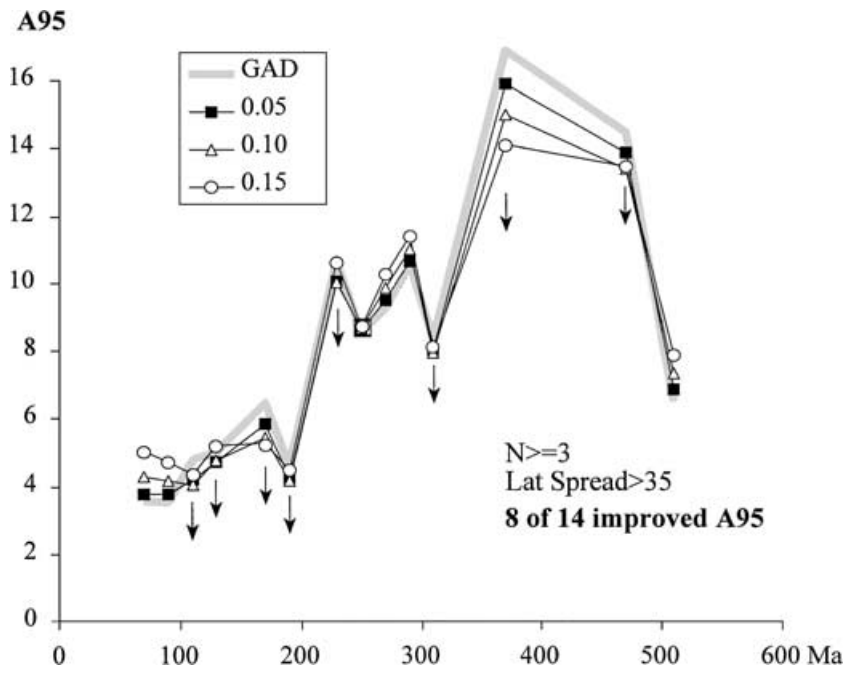
Figure 10. A95 for Gondwana mean poles as a function of different G3 contributions. Arrows indicate time intervals when A95 is reduced when G3 contributions are taken into account.
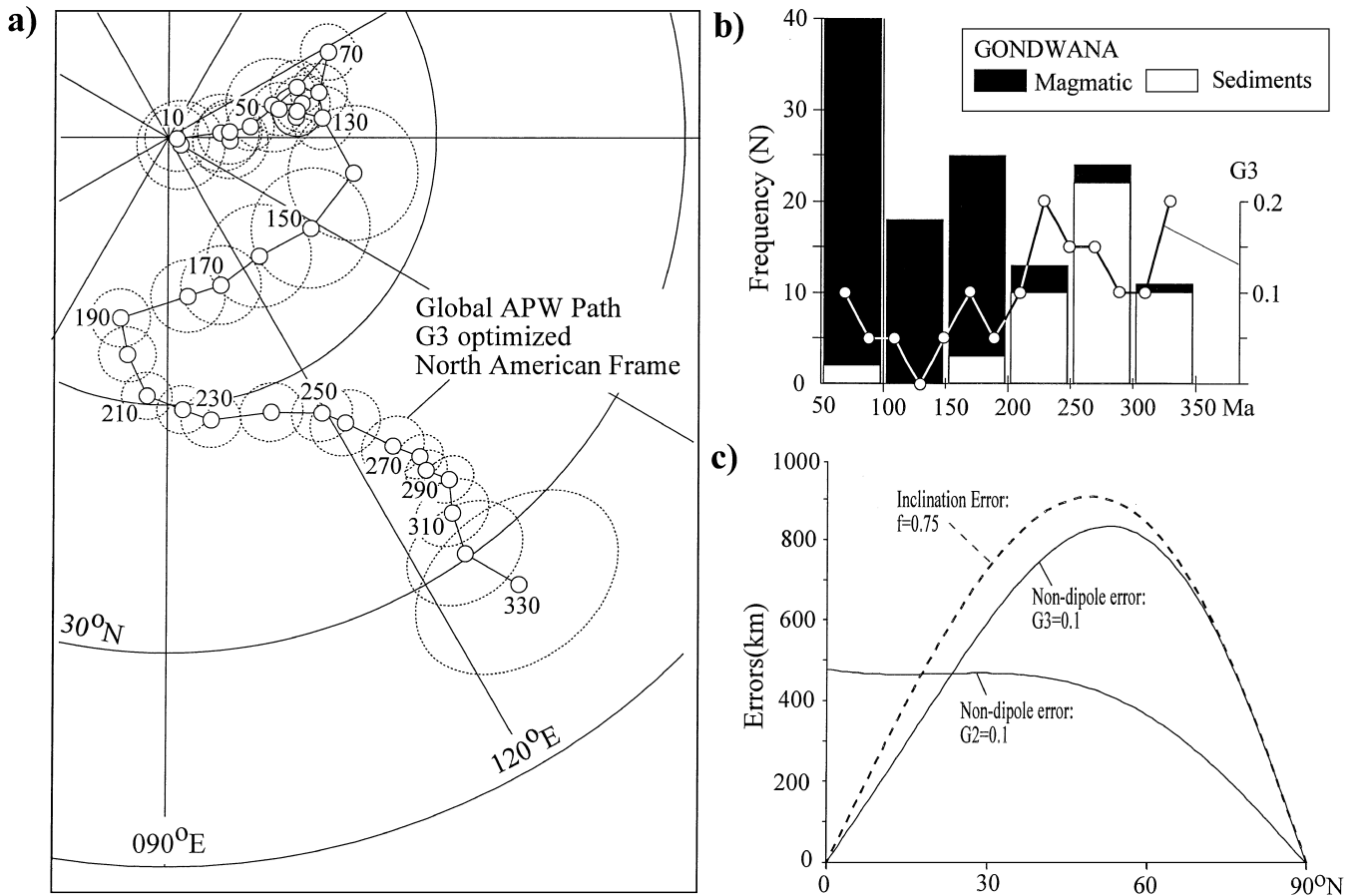
Figure 11. (a) G3 optimized global APW path for the last 330 Ma (Table 6). We used a flat G3 = 0.08 value for the Tertiary (Torsvik *et al.* 2001a). (b) Frequency versus age diagram for magmatic and sedimentary poles from Gondwana. Note the large input of sedimentary poles for ages >200 Ma when G3 is apparently very high (0.1–0.2). (c) Predicted latitudinal errors in palaeomagnetic reconstructions owing to non-dipole field (examples show G2 = 0.1 and G3 = 0.1) or inclination shallowing in sediments (f = 0.75).

Table 6. Running mean global and non-dipole field-corrected APW path in North American coordinates (see Fig. 11a and text); age ± 10 Ma.

Age	Plat	Plon	A95	*N*
0	88.4	148.73	4.9	11
10	89.04	172.94	3.61	15
20	84.19	185.23	4.25	18
30	83.16	177.26	4.15	20
40	83.21	185.5	3.55	18
50	80.88	187.79	2.64	28
60	74.74	201.49	2.97	37
70	69.95	208.33	3.08	31
80	72.63	196.78	3.17	33
90	74.77	194.35	3.13	31
100	77.96	197.52	5.13	11
110	77.4	194.58	2.9	16
120	75.5	191.63	2.74	24
130	72.81	187.39	3.47	17
140	69.06	169.23	7.34	9
150	71.28	147.65	6.6	16
160	73.44	127.65	5.72	14
170	72.61	109.81	4.4	19
180	72.26	97.14	4.07	23
190	69.25	75.23	3.27	28
200	65.38	79.44	3.13	34
210	60.98	85.42	2.72	29
220	59.43	93.23	2.79	30
230	57.91	98.82	3.19	28
240	57.03	110.67	3.37	35
250	54.47	119.21	3.26	41
260	52.08	121.88	3.78	31
270	46.64	126.11	3.39	35
280	43.68	128.32	2.5	53
290	41.88	127.86	2.25	45
300	39.27	129.44	2.67	26
310	35.73	127.17	3.87	24
320	30.57	125.57	6.04	13
330	23.21	128.13	10.42	5

of G3, but others become worse. Furthermore, A95 changes are not statistically significant, leading us to conclude that this aspect of our analysis is inconclusive.

6 A GLOBAL NON-DIPOLE FIELD-CORRECTED APW PATH (0–330 Ma)

We now combine all Gondwana and Laurussia poles from 330 Ma and younger. We also upgraded the Laurussia data base (Torsvik *et al.* 2001) with poles younger than 40 Ma (Si & Van der Voo 2001). We then recalculated all poles with optimal time-dependent G3 contributions (from Fig. 8b) and the resultant APW is shown in Fig. 11(a) (Table 6). For Tertiary times we used a flat G3 value of 0.08 (Torsvik *et al.* 2001c). The G3-adjusted APW path represents our best estimate of global APW and does not violate Pangea-A reconstructions. The global APW path strictly applies from the formation to the breakup of Pangea, but combined with Jurassic and younger magnetic anomaly fits we can also construct a 'synthetic' global APW path since the demise of the Pangea Supercontinent.

The global APW must be regarded with caution because the complexity of the ancient geomagnetic field is not known in detail. In addition, inclination errors in sediments could play an important role (see later). This notwithstanding, the path is considered better than any GAD-based APW paths. We incorporate only octupole fields because the Pangea problem cannot be rectified with long-term quadrupole contributions. We have also recalculated the Gondwana spline APW path with G3 contributions and we used a flat G3 value of 0.2 for times older than 330 Ma (Table 3, Fig. 5a). The latitude versus time diagram (Fig. 6), as expected, demonstrates that the G3 path reveals overall higher latitudes than the GAD path. The G3-optimized APW path for Gondwana closely tracks that calculated from a GAD model (Fig. 5a) but there are notable differences that will produce different paleogeographic positions for Gondwana.

7 TIME-DEPENDENT G3 FIELDS OR INCLINATION ERROR?

Kent & Smethurst (1998) suggested that large G3 values (0.25) in Precambrian–Palaeozoic times (absent in their Mesozoic analysis) were related to growth of the inner core, and that by the Early Mesozoic (250 Ma) the inner core had grown to a critical threshold size that had
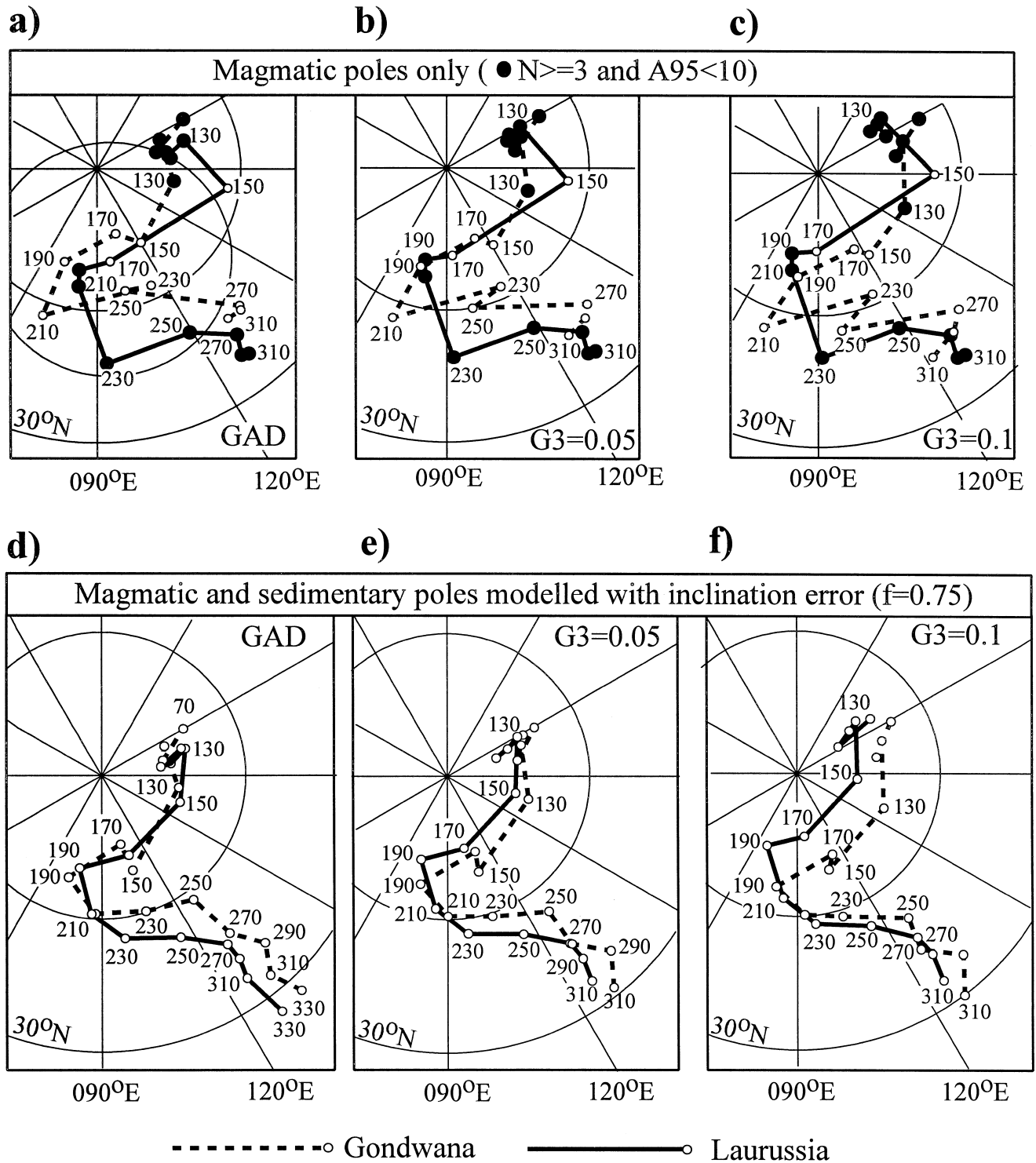
Figure 12. APW paths for Gondwana and Laurussia exclusively based on magmatic poles (a–c) or on a combination of sedimentary poles corrected for inclination error ($f = 0.75$) and magmatic poles (d–f). Diagrams from left to right show paths based on GAD, G3 = 0.05 and G3 = 0.1 models.

a stabilizing effect on the geodynamo. It is clear, however, that significant octupole contributions exist in the Mesozoic–Cenozoic record, although our analysis suggests that at around 210 Ma the geomagnetic field may have become more dipolar. If the geomagnetic field is becoming increasingly more dipolar with time, then Proterozoic (e.g. Rodinia) reconstructions must be treated with great caution. G3 values of, for example, 0.3 will cause an error of around 2000 km at intermediate latitudes. Recall that octupole fields are antisymmetric, hence the errors would be similar in both hemispheres. This is why Pangea-A reconstructions can be rectified with G3 fields and *not* by quadrupole fields (Van der Voo & Torsvik 2001), because the latter are symmetric about the equator.

Prior to the Late Triassic–Early Jurassic (*c.* 210 Ma), 10 per cent or higher octupole field contributions are needed to rectify the Pangea-A problem, whilst lower values are indicated after this time. However, this apparent decline in non-dipole fields with time could be an illusion caused by a higher ratio of sedimentary poles in the Gondwana Late Palaeozoic–Triassic data set (Fig. 11b). Inclination error in sediments is a well-known phenomenon (e.g. Rochette & Vandamme 2001, and references therein); it is latitude dependent and antisymmetric, and the effect therefore closely mimics errors produced by G3 fields of the same sign as the dipole field. The degree of inclination shallowing depends on several factors, e.g. rock type (terrestrial red beds versus deep marine sediments) and remanence acquisition/shallowing mode (detrital (DRM) versus compaction-induced). Inclination shallowing is commonly predicted from $\tan(inc_{observed}) = f \tan(inc_{field})$, where inc is the inclination and f is the degree of inclination error. As an example, realistic f values of around 0.75 will produce latitudinal errors that are comparable to the effects of G3 ratios of 0.1 (Fig. 11c).

Van der Voo & Torsvik (2001) also found persistent latitudinal errors in the Laurussian data set when magmatic rocks were analysed separately, leading them to conclude that octupole fields had to be held responsible, instead of inclination shallowing. In the Gondwana data base there are few sedimentary poles younger than 200 Myr, whilst the opposite is true for <200 Ma (Fig. 11b). This is the threshold time where high octupole contributions (often 15–20 per cent) must be invoked to rectify the Pangea-A problem, and it is therefore appropriate to consider the inclination error as an alternative mechanism behind the apparent increase in G3. We first tested this issue by comparing APW paths exclusively based on magmatic poles (Figs 12a–c) and we notice that Jurassic mean poles are reasonable matches, but the Permo-Carboniferous misfits are clearly recognized with a GAD model. As in Fig. 7(b), a G3 of 0.05 is better for most of the Jurassic, whilst G3 = 0.1 leads to a reasonable overlap in the Permo-Carboniferous sections. Recall that G3 values of 0.15–0.2 were required in earlier analysis (Figs 7e–f and 11b) but the scarcity of magmatic poles from Gondwana (i.e. only six poles between 200–300 Ma) makes this analysis semi-quantitative. In Fig. 12(d) we recalculated all sedimentary poles with an average f value of 0.75; we then combined these 'corrected' sedimentary poles with magmatic poles and subsequently added G3 fields in 0.05 increments (Figs 12e and f). From this example, it is clear that only G3 >0.1 produces a good fit for the Permo-Carboniferous section, and this leads us to believe that an average G3 of 0.1 is necessary to rectify the Pangea-A problem, even when the inclination error in sediments is incorporated as an additional factor. Thus, given that the error versus latitude for inclination shallowing and G3 fields are similar (Fig. 11c), the optimized global APW path (Fig. 11a) is considered as a good proxy that corrects for G3 contributions as well as potential inclination errors. In detail, however, incorporation of inclination errors seriously complicates APW analysis because f-values depend on rock type, sedimentary environment, as well as site latitude.

8 CONCLUSIONS

(1) Based on a comprehensive re-examination of palaeomagnetic data from the Gondwana supercontinent we have constructed a revised APW path from its formation at *c.* 550 Myr until its demise in the Jurassic and beyond.

(2) When the Gondwana APW path is compared with that of Laurussia it is obvious that a Pangea-A configuration is not possible prior to the Mid-Jurassic (*c.* 170 Ma) unless we invoke considerable non-dipole (G3) field contributions. Latitude errors produced by inclination shallowing alone cannot be held responsible, although they may magnify the discrepancies.

(3) G3 fluctuates, but there is a decreasing trend with time that intuitively could be related to inner core growth and a stabilization of the geodynamo. However, this could be an illusion and be caused by additional inclination errors owing to the high ratio of sedimentary/magmatic poles prior to the Early Triassic.

(4) We have calculated a combined Laurussia–Gondwana APW path that represents the best available estimate of global APW. This APW path accounts for latitudinal errors produced by G3 fields (or equivalently, by inclination shallowing), and when combined with relative fits, it describes a self-consistent plate tectonic model for the last 330 Myr that complies with Pangea-A reconstructions.

REFERENCES

Athavale, R.N., Hansraj, A. & Verma, R.K., 1972. Palaeomagnetism and age of Bhander and Rewa sandstones from India, *Geophys. J. R. astr. Soc.,* **28,** 499–509.

Bachtadse, V. & Briden, J.C., 1990. Palaeomagnetic constraints on the position of Gondwana during Ordovician to Devonian times, in *Palaeozoic Palaeogeography and Biogeography,* Vol. 12, pp. 43–48, eds McKerrow, W.S. & Scotese, C.R., Geol. Soc. Lond. Mem.

Cocks, L.R.M. & Torsvik, T.H., 2002. Earth Geography from 500 to 400 million years ago: a faunal and palaeomagnetic review, *J. Geol. Soc. Lond.* (in press).

Coffin, M.F. & Rabinowitz, P.D., 1988. Evolution of the conjugate East African–Madagascan margins and the western Somali Basin, *Geol. Soc. Am. Spec. Paper,* **226**, 78.

Derder, M.E.M., Smith, B., Henry, B., Yelles, A.K., Bayou, B., Djellit, H., Ouali, R.A. & Gandriche, H., 2001. Juxtaposed and superimposed paleomagnetic primary and secondary components from the folded middle Carboniferous sediments in the Reggabe Basin (Sahara craton, Algeria), *Tectonophysics,* **332**, 403–422.

Gradstein, F.M., Agterberg, F.P., Ogg, J.G., Hardenbol, J., Van Veen, P., Thierry, J. & Huang, Z., 1995. A Triassic, Jurassic and Cretaceous time scale, in *Geochronology, Time Scales and Global Stratigraphic Correlation*, Vol. 54, pp. 95–126, eds Berggren, W.A., Kent, D.V., Aubry, M.P. & Hardenbol, J., Spec. Publ. Soc. Sed. Geol. Tulsa.

Grunow, A., 1999. Gondwana events and palaeogeography: a palaeomagnetic review, *J. African Earth Sci.,* **28,** 53–69.

Grunow, A.M. & Encarnación, J., 2000. Terranes or Cambrian polar wander: new data from the Scott Glacier area, Transantarctic Mountains, Antarctica, *Tectonics,* **19,** 168–181.

Kent, D.V. & Van der Voo, R., 1990. Palaeozoic palaeogeography from palaeomagnetism of the Atlantic-bordering continents, in *Palaeozoic Palaeogeography and Biogeography,* Vol. 12, pp. 49–56, eds McKerrow, W.S. & Scotese, C.R., Geol. Soc. Lond. Mem.

Kent, D.V. & Smethurst, M.A., 1998. Shallow bias of paleomagnetic inclinations in the Paleozoic and Precambrian, *Earth planet. Sci. Lett.,* **160,** 391–402.

Klootwijk, C.T., 1996. Phanerozoic configurations of greater Australia: evolution of the north west shelf. Part two: Palaeomagnetic and geological constraints on reconstructions, *Australian Geol. Surv. Org. Rec.,* **52,** 85.

Lottes, A.L. & Rowley, D.B., 1990. Reconstruction of the Laurasian and Gondwana segments of Permian Pangaea, in *Palaeozoic Palaeogeography and Biogeography*, Vol. 12, pp. 383–395, eds McKerrow, W.S. & Scotese, C.R., Geol. Soc. Lond. Mem.

McElhinny, M.W. & Lock, J., 1996. IAGA paleomagnetic databases with Access, *Surv. Geophys.,* **17,** 575–591.

McElhinny, M.W., McFadden, P.L. & Merrill, R.T., 1996. The time-averaged paleomagnetic field 0–5 Ma, *J. geophys. Res.,* **101,** 25 007–25 027.

McElhinny, M.W., Powell, C.McA. & Pisarevsky, S.A., 2002. Paleozoic terranes of eastern Australia and the drift of Gondwana, *Tectonophysics,* (in press).

Meert, J.G. & Van der Voo, R., 1997. The assembly of Gondwana 800–550 Ma, *J. Geodynamics,* **23,** 223–235.

Meert, J.G., Nedelec, A., Hall, C., Wingate, M.T.D. & Rakotondrazafy, M., 2001. Paleomagnetism, geochronology and tectonic implications of the Cambrian-age Carion granite, Central Madagascar, *Tectonophysics,* **340,** 1–21.

Morel, P. & Irving, E., 1981. Palaeomagnetism and the evolution of Pangaea, *J. geophys. Res.,* **86,** 1858–1872.

Müller, R.D., Royer, J.Y. & Lawver, L.A., 1993. Revised plate motions relative to the hotspots from combined Atlantic and Indian Ocean hotspot tracks, *Geology,* **21,** 275–278.

Müller, R.D., Roest, W.R., Royer, J.-Y., Gahagan, L.M. & Sclater, J.G., 1997. Digital isochrons of the world's ocean floor, *J. geophys. Res.,* **102,** 3211–3214.

Muttoni, G., Kent, D.V. & Channell, J.E.T., 1996. Evolution of Pangea: paleomagnetic constraints from the Southern Alps, Italy, *Earth planet. Sci. Lett.,* **140,** 97–112.

Rakotosolofo, N.A., Torsvik, T.H., Eide, E.A., Ashwal, L.D. & de Wit, M.J., 1999. The Karoo Supergroup revisited and Madagascar–Africa fits, *J. African Earth Sci.,* **29,** 135–151.

Rochette, P. & Vandamme, D., 2001. Pangea B: an artifact of incorrect paleomagnetic assumptions?, *Ann. Geofis.,* **44,** 649–658.

Schneider, D.A. & Kent, D.V., 1990. Testing models of the Tertiary paleomagnetic field, *Earth planet. Sci. Lett.,* **101,** 260–271.

Scotese, C.R. & Barrett, S.F., 1990. Gondwana's movement over the South Pole during the Palaeozoic: evidence from lithological indicators of climate, in *Palaeozoic Palaeogeography and Biogeography,* Vol. 12, pp. 75–85, eds McKerrow, W.S. & Scotese, C.R., Geol. Soc. Lond. Mem.

Si, J. & Van der Voo, R., 2001. Too-low magnetic inclinations in Central Asia: an indication of a long-term tertiary non-dipole field?, *TerraNova,* **13,** 471–478.

Smith, A.G., 1999. Gondwana: its shape, size and position from Cambrian to Triassic times, *J. African Earth Sci.,* **28,** 71–97.

Storetvedt, K.M., Mitchell, J.G., Abranches, M.C., Maaloe, D. & Robin, G., 1992. The coast-parallel dolerite dykes of east Madagascar: age of intrusion, remagnetization and tectonic aspects, *J. African Earth Sci.,* **15,** 237–249.

Storey, M., Mahoney, J.J., Saunders, A.D., Duncan, R.A., Kelley, S.P. & Coffin, M.F., 1995. Timing of hot spot-related volcanism and the break-up of Madagascar and India, *Science,* **267,** 852–855.

Torcq, F., Besse, J., Vaslet, D., Marcoux, J., Ricou, L.E., Halawani, M. & Basahel, M., 1997. Paleomagnetic results from Saudi Arabia and the Permo-Triassic Pangea configuration, *Earth planet. Sci. Lett.,* **148,** 553–567.

Torsvik, T.H., Smethurst, M.A., Meert, J.G., Van der Voo, R., McKerrow, W.S., Brasier, M.D., Sturt, B.A. & Walderhaug. H.J., 1996. Continental break-up and collision in the Neoproterozoic and Palaeozoic: a tale of Baltica and Laurentia, *Earth Sci. Rev.,* **40,** 229–258.

Torsvik, T.H., Tucker, R.D., Ashwal, L.D., Eide, E.A., Rakotosolofo, N.A. & de Wit, M.J., 1998. Late Cretaceous magmatism in Madagascar: palaeomagnetic evidence for a stationary Marion hotspot, *Earth planet. Sci. Lett.,* **164,** 221–232.

Torsvik, T.H., Tucker, R.F., Ashwal, L.D., Carter, L.M., Jamtveit, B., Vidyadharan, K.T. & Venkataramana, P., 2000. Late cretaceous India–Madagascar fit and timing of break-up related magmatism, *TerraNova,* **12,** 220–224.

Torsvik, T.H., Mosar, J. & Eide, E.A., 2001a. Cretaceous–tertiary geodynamics: a North Atlantic exercise, *Geophys. J. Int.* **146,** 850–867.

Torsvik, T.H., Carter, L.M., Ashwal, L.D., Bhushan, S.K., Pandit, M.K. & Jamtveit, B., 2001b. Rodinia refined or obscured: palaeomagnetism of the Malani igneous suite (NW India), *Precambrian Res.,* **108,** 319–333.

Torsvik, T.H., Van der Voo, R., Meert, J.G., Mosar, J. & Walderhaug, H.J., 2001c. Reconstructions of the continents around the North Atlantic at about the 60th parallel, *Earth planet. Sci. Lett.,* **187,** 55–69.

Tucker, R.D. & McKerrow, W.S., 1995. Early Palaeozoic chronology: a review in light of new U-Pb zircon ages from Newfoundland and Britain, *Can. J. Earth Sci.,* **32,** 368–379.

Tucker, R.D., Bradley, D.C., Ver Straeten, C.A., Harris, A.G., Ebert, J.R. & McCutcheon, S.R., 1998. New U-Pb zircon ages and the duration and division of Devonian time, *Earth planet. Sci. Lett.,* **158,** 175–186.

Van der Voo, R., 1993. *Paleomagnetism of the Atlantic, Tethys and Iapetus Oceans,* p. 411, Cambridge University Press, Cambridge.

Van der Voo, R. & Torsvik, T.H., 2001. Evidence for Permian and Mesozoic non-dipole fields provides an explanation for the Pangea reconstruction problems, *Earth planet. Sci. Lett.,* **187,** 71–81.

APPENDIX A: RECALCULATING PALEOMAGNETIC POLES WITH G2 AND G3 CONTRIBUTIONS

In order to use one's 'favourite' routine to calculate palaeomagnetic poles based on a geocentric axial dipole model, we list a Visual Basic routine below that calculates a new inclination (IncG23) based on the observed inclination (IncObserved) and the amount of G2 and G3 contributions. This new inclination can be fed directly into an existing GAD routine. The routine uses numerical iteration (the accuracy is set to $0.1°$ in the code below).

'Input variables:
'IncObserved is the mean inclination for a specific study
'G2, G3 are zonal G2 and G3 contributions (given as 0.05 (= 5 *per cent*), 0.1 (= 10 *per cent*), *etc.*)

'Output variable:
'IncG23 which is fed into a GAD-based pole calculation routine

pie = 3.14159/180 $'conversion factor to radians$

```
FOR a = 0 To 180 STEP 0.1        'co-latitude loop in 0.1° increments
i = a * pie                      'convert from degrees to radians
'expression for G1 (axial dipole),   G2 (quadrupole) and G3 (octupole)
'see Schneider & Kent (1990)
TanIa = 2 * COS(i) + G2 * (4.5 * COS(i) ∧ 2 − 1.5) + G3 * (10 * COS(i) ∧ 3 − 6 * COS(i))
TanIb = SIN(i) + G2 * (3 * COS(i) * SIN(i)) + G3 * (7.5 * COS(i) ∧ 2 * SIN(i) − 1.5 * SIN(i))
Tani = TanIa/TanIb
G23INC = ATN(tani)/pie        'inclination with G3 and G2 contributions

IF ABS (IncObserved − G23INC) <=0.1 THEN    'we have a match
'calculate inclination now without G2 and G3 for same co-latitude
TanIa = 2*COS(i)
TanIb = SIN(i)
Tani = TanIa/TanIb
IncG23 =ATN(tani)/pie    'new inclination
'Insert one's own paleomagnetic pole calculation routine (GAD-based) here
'by substituting Inc G23 for IncObserved
STOP
END IF
NEXT a
```

EXAMPLE:

DecObserved =342°, IncObserved = 58°, SiteLatitude = 61.3°N, SiteLongitude = 5.0°E

$\Longrightarrow$ Paleomagnetic pole (GAD): 64.8°N–219.5°E

Paleomagnetic pole (G3 = 0.1): 71.5°N–227.5°E (IncG23 = 64.2°)